Check for updates

ADVANCED MATERIALS
www.advmat.de

Aqueous Organic Batteries Using the Proton as a Charge Carrier

*Mangmang Shi, Pratteek Das, Zhong-Shuai Wu, Tie-gen Liu, and Xiaoyan Zhang**

Benefiting from the merits of low cost, nonflammability, and high operational safety, aqueous rechargeable batteries have emerged as promising candidates for large-scale energy-storage applications. Among various metal-ion/non-metallic charge carriers, the proton (H^+) as a charge carrier possesses numerous unique properties such as fast proton diffusion dynamics, a low molar mass, and a small hydrated ion radius, which endow aqueous proton batteries (APBs) with a salient rate capability, a long-term life span, and an excellent low-temperature electrochemical performance. In addition, redox-active organic molecules, with the advantages of structural diversity, rich proton-storage sites, and abundant resources, are considered attractive electrode materials for APBs. However, the charge-storage and transport mechanisms of organic electrodes in APBs are still in their infancy. Therefore, finding suitable electrode materials and uncovering the H^+-storage mechanisms are significant for the application of organic materials in APBs. Herein, the latest research progress on organic materials, such as small molecules and polymers for APBs, is reviewed. Furthermore, a comprehensive summary and evaluation of APBs employing organic electrodes as anode and/or cathode is provided, especially regarding their low-temperature and high-power performances, along with systematic discussions for guiding the rational design and the construction of APBs based on organic electrodes.

1. Introduction

The gravity of the approaching energy crisis, such as the dwindling supplies of fossil fuels, and the undeniable environmental impact resulting from their burning for centuries, has become more noticeable in recent times. This has stimulated researchers to explore alternative sources such as solar, wind, and hydro-energy, among others, due to their cleanliness and sustainability.[1–3] Therefore, there is an increasing demand for advanced electrochemical energy storage/conversion systems such as various metal-ion batteries and supercapacitors to fully utilize intermittent energies and realize efficient energy conversion.[4–9] Safety concerns about organic electrolyte-based batteries have spurred the search for rechargeable aqueous batteries especially in grid-scale energy-storage applications, due to the merits of low cost, non-flammability, and high operational safety.[1,10] In addition, aqueous media shows a higher ionic conductivity (≈1 S cm^{-1}) than non-aqueous media, which endows aqueous batteries with excellent rate performance.[11] Charge carriers, as a core component of aqueous batteries, directly determine their electrochemical nature and energy-storage behaviors.[12] Over the past decade, the research interests and achievements in aqueous batteries based on metal-ion charge carriers (e.g., Li^+, Na^+, K^+, Zn^{2+} Mg^{2+}, and Al^{3+})[13–18] have surged for their high energy density, high volumetric energy density, and excellent stability.[19] Despite these great features, metal-ion aqueous batteries have a poor ability to deliver instantaneous power output due to the sluggish ion-transport caused by the large solvation radius and strong electrostatic interactions.[20] Fortunately, non-metallic charge carriers (e.g., H^+, NH_4^+, and OH^-)[21–23] with a lighter mass and a smaller ionic radius, possess faster kinetics in aqueous batteries. However, compared with the flourishing metal-ion charge carriers, the development of

M. Shi, X. Zhang
Department of Chemistry and Chemical Engineering
Chalmers University of Technology
Kemigården 4, Göteborg SE-412 96, Sweden
E-mail: xiaoyan.zhang@chalmers.se

M. Shi
School of physics
Xi'an Jiaotong University
Xi'an 710049, China

P. Das, Z.-S. Wu
State Key Laboratory of Catalysis
Dalian Institute of Chemical Physics
Chinese Academy of Sciences
457 Zhongshan Road, Dalian 116023, China

T.-gen Liu
The Ministry of Education Key Laboratory of Optoelectronic Information Technology
Tianjin University
Tianjin 300072, China

The ORCID identification number(s) for the author(s) of this article can be found under https://doi.org/10.1002/adma.202302199

© 2023 The Authors. Advanced Materials published by Wiley-VCH GmbH. This is an open access article under the terms of the Creative Commons Attribution License, which permits use, distribution and reproduction in any medium, provided the original work is properly cited.

DOI: 10.1002/adma.202302199

aqueous batteries based on non-metallic charge carriers need to be further improved.

As one of the non-metallic charge carriers, the proton, has received much attention, for its obvious advantages in terms of: a) hydrogen element is abundantly available on earth, ensuring the sustainability and affordability of proton batteries;[24] b) proton possesses a low molar mass, leading to a higher capacity of the electrode;[25] c) the smaller hydrated ion radius of H^+ (0.228 nm) can not only favor to the kinetics of H^+ diffusion but also can reduce the volume expansion of electrode materials during the deintercalation/intercalation process.[26] Inspired by the fascinating proton chemistry, many inorganic and organic type materials with high performance have been explored to meet the rapid development of APBs. In general, during the selection of electrode materials, their intrinsic properties, such as excellent electrochemical performance, good chemical stability, non-toxic nature, and wide operation voltage window, should be taken into consideration.[11] Along these lines, compared with traditional inorganic compounds, organic electrodes are very promising candidates in energy-storage devices thanks to their low cost, structural diversity, high theoretical capacity, and rich H^+-storage sites.[10]

However, the application and understanding of charge-storage/transport mechanisms of organic electrodes in APBs are still in their infancy. Therefore, selecting suitable electrode materials and uncovering the H^+-storage mechanisms are significantly important for the practical applications of organic materials in APBs. Herein, we systematically review the latest research progress on organic materials such as conducting polymers/small molecules (anode and cathode) and the energy-storage mechanisms in APBs. In addition, the APB systems based on organic electrodes (organic//inorganic electrode batteries or all-organic batteries) and the relationship among different APBs are discussed as well. This review provides guidance on the future development of organic materials in APBs.

2. Main Discussions

2.1. Characterization Techniques

2.1.1. Structural and Morphological Characterizations

Generally, nuclear magnetic resonance (NMR) is an effective method to confirm the structure and the purity of as-synthesized organic molecules including small molecules and polymers. However, the practical applications of these organic molecules especially small molecules are still hindered by the low conductivity and the inevitable dissolution into electrolytes during charge–discharge processes.[27] There are two feasible approaches to solve this issue: 1) polymerization of small organic compounds via condensation reactions or oxidative polymerization: for example, polyanthraquinone (PAQ) can be synthesized by coupling of anthraquinone (AQ) rings via a simple one-step condensation polymerization reaction. The PAQ-based electrode shows a more stable cycling stability than the one of AQ for Li storage;[28] 2) the construction of organic molecule electrodes (OMEs) via integration with conductive carbon substrates. As a typical carbon material, graphene (a single-layer of sp^2 carbon), with the merits of large specific surface area, high electrical conductivity, and excellent capacitive performance, has been used as a common conductive substrate to adsorb organic molecules.[29–36] Generally, organic molecules can be immobilized on the defects or residual groups of graphene sheets via covalent bonding, which can inevitably interrupt the conjugated system of graphene resulting in the conversion of sp^2 to sp^3 hybridized carbon.[37,38] Moreover, non-covalent functionalization provides a simple and economic approach to attach organic molecules on the surface of graphene through van der Waals forces, dispersive, hydrophobic, or electrostatic interactions (e.g., π–π stacking), in which the sp^2 network of graphene may not be disrupted ensuring a high electrical conductivity of graphene.[39,40] Interestingly, compared with the location of the C=O group and the C–H bonds in Fourier-transform infrared (FT-IR) spectra for the pure organic molecules, the stretching vibration of the C=O group and the C–H bonds in organic-based composites show a shift, indicating the integration of organic molecules and conductive carbon substrates via non-covalent π–π interactions.[41–44] Furthermore, Wang's group shows that the adsorption energy can reach 29.9 kJ mol^{-1} with the anthraquinone-2-sulfonate anion parallel to the bare graphene sheet, further demonstrating the existence of non-covalent π–π interactions.[45]

Moreover, the theoretical specific capacity (Q_{theo}, mAh g^{-1}) of organic electrodes can be obtained from the following formula.[46]

$$Q_{\text{theo}} = \frac{nF}{3.6M_{\text{w}}} \tag{1}$$

where n represents the number of transferred electrons during the charging/discharging process, F is the Faraday constant (C mol^{-1}), and M_w is the molecular mass (g mol^{-1}). According to this equation, pyrene-4,5,9,10-tetraone (PTO/PYT) molecules with four carbonyl redox groups can transfer four electrons per molecule, showing a high theoretical capacity of ≈400 mAh g^{-1}.[47] In fact, the PYT-based electrode delivers a specific capacity of 300 mAh g^{-1} at a current density of 0.1 A g^{-1} in an aqueous zinc battery[48] and possesses a reversible specific capacity of 208 mAh g^{-1} at a current density of 0.16 mA cm^{-2} in APB,[49] which are lower than the theoretical capacity (≈400 mAh g^{-1}). Many factors, such as electrical conductivity, specific surface area, morphology, and chemical compositions, determine the practical specific capacity of organic electrodes. Therefore, it is necessary to characterize the morphology, microstructure, and chemical compositions of OMEs, using scanning electron microscopy (SEM), transmission electron microscopy (TEM), and X-ray photoelectron spectroscopy (XPS), which are important tools for the characterization of electrochemical performance. For example, the SEM images demonstrated that hexaazatrinaphthalene-quione (HATNQ) possesses a layered nano morphology.[50] The corresponding high-resolution TEM image of the HATNQ reveals the clear lattice fringes with a spacing of 0.33 nm, which may be ascribed to the π–π stacking.

2.1.2. Electrochemical Measurements

The conventional three-electrode system is carried out to test the electrochemical performance of individual electrodes. Cyclic voltammetry (CV), galvanostatic charge/discharge (GCD), and electrochemical impedance spectroscopy (EIS) performed on an

© 2023 The Authors. Advanced Materials published by Wiley-VCH GmbH

15214095, 2023, 42, Downloaded from https://onlinelibrary.wiley.com/doi/10.1002/adma.202302199 by Dalian Institute Of Chemical, Wiley Online Library on [24/01/2024]. See the Terms and Conditions (https://onlinelibrary.wiley.com/terms-and-conditions) on Wiley Online Library for rules of use; OA articles are governed by the applicable Creative Commons License

electrochemical workstation are common characterization techniques to analyze the energy-storage mechanism and examine the capacitance of electrode materials. Meanwhile, it is an effective strategy to distinguish capacitive, pseudocapacitive, and battery-type materials according to the CV and GCD responses of electrode materials.[51,52] Typically, a CV experiment is used to analyze electrochemical kinetics, reveal details on the charge-storage process, and quantify the contributions of diffusion-controlled (battery-like) and surface-controlled (capacitor-like) processes.[53]

2.1.3. Mechanism Characterization Techniques

While the abovementioned electrochemical analysis techniques can help to directly speculate the energy-storage mechanism, it is still highly desired to have more direct evidence by monitoring structural changes of electrode materials during charging/discharging processes. Hence, in situ/ex situ Raman spectroscopy, diffuse reflectance infrared Fourier transform spectroscopy, X-ray diffraction (XRD), SEM, and TEM characterizations are conducted to provide insights into the redox process and unravel the structure-property relationship. For example, in order to deeply understand the proton redox process in the redox-active polymer with diquinoxalino-phenazine (PDPZ) as the structural unit, in situ Raman investigation and FT-IR measurements were carried out.[54] The results of in situ Raman investigation show that the characteristic peak of the C=N bond gradually disappears and the peak of the C–N bond appears during the discharge process. Subsequently, the C=N bond recovers and the C–N bond disappears during the charge process, further confirming the highly reversible protonation/deprotonation process of organic electrode materials with PDPZ as the structural unit. In situ FT-IR measurement shows that the peak of the N–H bond emerges, demonstrating that with the proton insertion, the C=N bond of PDPZ transforms into a C–N bond and an N–H bond. In addition, an in situ Raman investigation was performed to gain a deeper understanding of the proton-storage process of hexaazatrinaphthalene (HATN).[55] Obviously, with the insertion of protons, the C=N bond (1420 cm^{-1}) in the HATN molecule gradually disappears, while the C–N (1390 cm^{-1}) bond and the N–H bond (1521 cm^{-1}) simultaneously emerge. Similarly, during the charging process, the disappearance of the C–N/N–H bonds and the reinstatement of the C=N bond further confirm the high redox reversibility of the HATN during the proton insertion/extraction process. As for the N-containing organic compounds, the ex situ XPS spectra of N1s of the electroactive organic building blocks (HATN) also indicate the reversible transformation from the –C=N– group to the –C–N– group.[56]

In situ XRD patterns can be used to confirm the transformation of the crystal structures of organic compounds during charge/discharge processes. For example, with the insertion of H^+, the crystalline structure of tetramethylquinone (TMBQ) undergoes changes accompanied by the formation of a new phase (tetramethyl-hydroquinone, TMHQ).[57] Notably, in mixed electrolytes (e.g., 2 M HBF_4 + 2 M $Mn(BF_4)_2$), it is often confusing whether manganese is involved in the reaction. The ex situ TEM-mapping images indicate that the H^+ can reversibly insert/extract in alloxazine (ALO) and Mn^{2+} is not involved in the above process.[58] Therefore, in practice, a variety of advanced in situ/ex situ tests are required to clarify the exact proton-storage mechanism.

2.1.4. Theoretical Calculations

As for the organic electrode materials, the insight into the relationship between energy levels of the lowest unoccupied molecular orbital (LUMO) and the highest occupied molecular orbital (HOMO) is favorable to the analysis of the energy-storage mechanism and the rational construction of the full-cell system. LUMO and HOMO energies of organic materials are an indicator of the ability to attract or release electrons, respectively.[59] Importantly, organic materials with a lower LUMO energy level imply higher electron affinity, leading to a higher reduction potential.[60] Therefore, the introduction of electron-withdrawing/donating groups into organic materials can adjust their LUMO energy levels, resulting in considerable output potential. Especially, the introduction of electron-withdrawing groups (e.g., -CN, -F, -Cl, and -Br) can significantly decrease the LUMO energy level of organic materials, resulting in a high output potential.[61] Due to the introduction of electron-donating/withdrawing groups, the LUMO energy level obtained from the DFT calculations of benzoquinone (BQ, –H), tetramethylbenzoquinone (TMBQ, $-CH_3$), and tetrachlorobenzoquinone (TCBQ, –Cl) follows the order of TMBQ > BQ > TCBQ.[57] Besides, the small energy gap between the LUMO and the HOMO demonstrates excellent electrical conductivity, which endows the electrode with an enhancement of the redox kinetics for H^+ uptake. Generally, the energy levels can be calculated from CV measurement and theoretical modeling. As for the dithieno[3,2-b:2′,3′-d]pyrrole (DTP), and the DTP modified with anthraquinone pendant (DTP-AQ) or the naphthoquinone pendant (DTP-NQ) monomers,[62] the HOMO/LUMO energy levels can be calculated to be −5.17/−3.51, −5.28/−3.72, and −5.29/−3.81 eV via the CV measurement in a 0.1 M $TBAPF_6$/MeCN. The variation trend matches well with the HOMO/LUMO energy levels (−5.14/−0.57, −5.44/−2.91, and −5.44/−3.27) calculated from the simulation. Apparently, as a supplementary technique, the simulation results show a slight deviation from experimental results. Therefore, during the simulation process, critical factors need to be continually optimized. Besides, the molecular electrostatic potential (MESP) can be calculated to infer the electrophilic (the negative MESP areas) and nucleophilic (the positive MESP areas) reaction-active sites.[63] Reaction-active sites with more negative MESP values show higher electronegativity, leading to their attraction to cations such as Zn^{2+}, Na^+, or H^+.[64] Therefore, MESP can provide speculation on the reactive sites for anions and cations, which can be beneficial in providing a deeper understanding of the exact proton-storage chemistry.

2.2. Electrode Preparation Methods

Traditionally, the as-obtained organic active materials, conductive additives (e.g., ketjen black, graphene, carbon nanotubes (CNTs), etc.), and binders (e.g., PVDF, PTFE, etc.) with a certain mass ratio are mixed in a solvent (e.g., *N*-methyl-2-pyrrolidone or ethanol) to obtain a homogeneous slurry. The

© 2023 The Authors. Advanced Materials published by Wiley-VCH GmbH

15214095, 2023, 42, Downloaded from https://onlinelibrary.wiley.com/doi/10.1002/adma.202302199 by Dalian Institute Of Chemical, Wiley Online Library on [24/01/2024]. See the Terms and Conditions (https://onlinelibrary.wiley.com/terms-and-conditions) on Wiley Online Library for rules of use; OA articles are governed by the applicable Creative Commons License

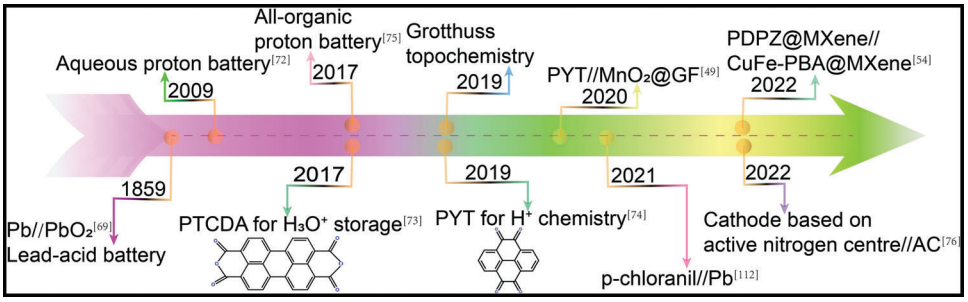

Figure 1. The timeline of organic electrodes for APBs.

slurry is cast onto a conductive current collector (e.g., carbon paper, graphite plate, titanium mesh, titanium foil, stainless-steel mesh, and glassy carbon electrode, etc.) and is further dried under vacuum to form the organic electrode for APBs. However, the introduction of electrochemically inactive components increases the total mass of devices and reduces the flexibility of electrodes. To address this issue, binder-free and self-supported electrodes have been developed such as phenothiazine on reduced graphene oxide (rGO) electrode,[65] covalent organic frameworks (COF)@rGO film,[66] diquinoxalinophenazine (6CN-DQPZ)@MXene electrode,[67] and flexible polyaniline@MXene.[68]

2.3. Proton as Charge Carriers and its Transport Mechanism

Proton as a charge carrier inherits the advantages of aqueous batteries such as the merits of rich reserves, low cost, and rapid kinetics of electrochemical storage. Meanwhile, finding suitable electrode materials is crucial for the development of APBs. **Figure 1** shows the timeline of APBs, demonstrating the milestones of organic molecules that have been used as electrode materials. As a matter of fact, the first APB can be dated back to the lead–acid batteries in 1859, where a H_2SO_4 solution supplied the proton source, and Pb and PbO_2 were used as the anode and the cathode, respectively.[69] The cell reaction based on conversion-type electrode materials can be described as follows.

$$PbO_2 + Pb + 2H_2SO_4 \rightleftharpoons 2PbSO_4 + 2H_2O \quad (2)$$

Later on, previous research work has already proven that H^+ can have a reversible insertion into metal oxides (e.g., RuO_2, and MnO_2).[70,71] In 2009, an emerging Zn//MnO_2 cell demonstrated that the proton insertion/extraction mechanism operates in a Li_2SO_4 electrolyte as well.[72] However, compared with the flourishing inorganic materials for proton storage, the development of organic materials is relatively slow. In 2017, Ji's group first demonstrated the crystalline 3,4,9,10-perylenetetracarboxylic dianhydride (PTCDA) can reversibly store the hydronium ions via ex situ X-ray diffraction.[73] Later, Wang's group reported that the PTO/PYT electrode can also store protons via a coordination reaction.[74] Interestingly, Sjödin's group designed an all-organic proton battery cell, which facilitates the development of organic electrodes for APBs.[75] A large potential difference between the electrodes is beneficial to a high energy density. Thus, various APBs employing organic and inorganic materials with a large potential difference as cathode and anode, have been proposed and developed.[49,54,57,76] Significantly, in the past decade, abundant redox-active organic molecules (e.g., sodium anthraquinone-2-sulfonate, phenothiazine, naphthalene diimide derivative, etc.) have been proven to show a high electrochemical performance in supercapacitors with H_2SO_4 solution as the electrolyte,[45,65,77,78] which can also be potential candidates for APBs.

Protons possess anomalously high ionic conductivity in a water environment, which unlocks rapid kinetics for APBs. The high ionic conductivity of protons originates from the prominent Grotthuss mechanism. In detail, protons can move between the adjacent H_2O lattice with the breaking and the formation of hydrogen bonds. Meanwhile, a series of similar displacements can be triggered via the hydrogen-bonding network, which endows protons with ultrafast migration along the H_2O chain.[79] Hence, the development of novel electrode materials for H^+ storage is very important to construct high-performance APBs.

2.4. Small Molecules/Polymers for H^+ Storage

Organic electrode materials are mainly composed of carbon(C), hydrogen (H), oxygen (O), and other elements (e.g., N, F, Cl, etc.), which have been successfully used for the metal-ion and non-metallic ion storage, showing the advantages of good chemical stability, non-toxic nature, and low cost.[80,81] Recently, owing to the substantial advancement in materials, electrochemical proton insertion into organic electrodes in aqueous media has been demonstrated to be feasible in battery/capacitor electrodes.[43,82] Therefore, a lot of organic electrode materials based on small molecules or polymers have served as the host materials for H^+ storage in APBs. As shown in **Figure 2**, according to the state change of redox-active units during the charging and discharging process, organic electrode materials can be classified into three types: n-type, p-type, and bipolar type.[46,83]

During the electrochemical reaction, n-type organic compounds including quinones, imides, phenazines, azos, and amides, first undergo a reversible reduction process to form a negatively charged state by accepting electrons. Conversely, p-type organic molecules such as imide, carbazole, and phenazine[84,85] derivatives show positively charged states by donating electrons. Bipolar-type organic molecules (e.g., polyaniline, polypyrrole, and conductive polythiophene skeleton) can simultaneously serve as electron acceptors and electron donors, which can be either reduced or oxidized.[86] In general, the majority of the molecular structures of the p-type organic

© 2023 The Authors. Advanced Materials published by Wiley-VCH GmbH

15214095, 2023, 42, Downloaded from https://onlinelibrary.wiley.com/doi/10.1002/adma.202302199 by Dalian Institute Of Chemical, Wiley Online Library on [24/01/2024]. See the Terms and Conditions (https://onlinelibrary.wiley.com/terms-and-conditions) on Wiley Online Library for rules of use; OA articles are governed by the applicable Creative Commons License

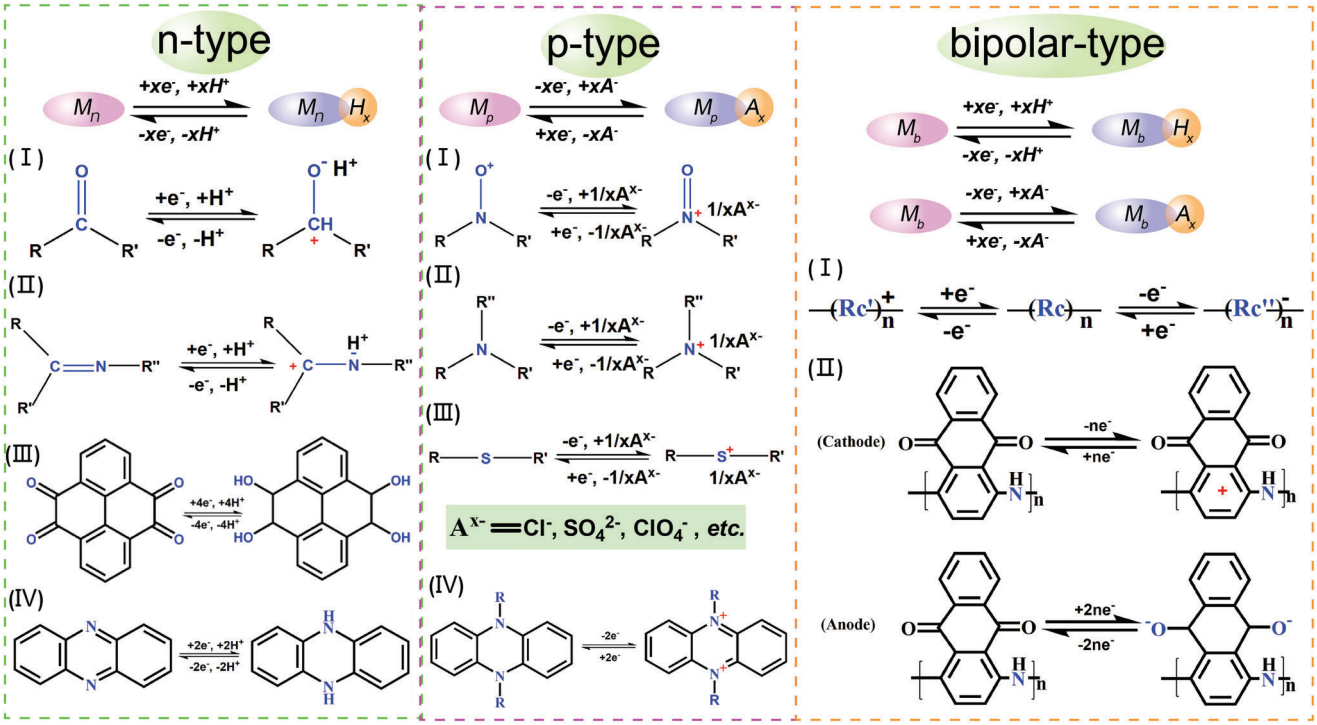

Figure 2. The proton-storage mechanisms of n-type, p-type, and bipolar-type organic electrodes in APBs.

electrode materials are redox-inactive. In contrast, n-type organic electrode materials possess rich active sites per weight, showing a higher specific capacity.[83]

The proton-storage mechanism in oxygen-containing and nitrogen-containing organic electrode materials (OEMs) is displayed in **Figure 3**. Obviously, the N and O heteroatoms are the main redox-active centers for reversible proton uptake/removal. The oxygen-containing OEMs (e.g., PYT), phenanthrenequinone (PQ),[87] and emodin molecules[88]) can undergo a reversible transformation from the –C=O bond to the –C–OH bond (Figure 3a,b). As for the nitrogen-containing OEMs (diquinoxalino[2,3-a:2′,3′-c]phenazine (HATN)) with the C=N groups, the proton can be reversibly stored in the C=N active sites to form the C–NH– bond during the discharge process.[89] Moreover, the HATN molecule possesses six N atoms as active centers, indicating the structural evolution from the HATN to the HATN-6H (Figure 3c). Interestingly, the bis(phenylamino)phenothiazin-5-ium iodide (PTD-1) with phenylimino groups and phenothiazine heterocyclic rings shows n/p-type reactions at a low potential and p-type reactions at a high potential.[90] As shown in Figure 3d, the I^- originated from the pristine PTD-1 sample and is replaced by SO_4^{2-} from the electrolyte. During the discharge process (from 1.1 to 0.1 V), the phenothiazine heterocyclic ring gains two electrons, accompanying the release of SO_4^{2-} (or I^-) and the proton coordination (step 1). When the voltage returns to 1.1 V, the SO_4^{2-} is extracted and the proton is released (step 2). Subsequently, during the further charge process, the phenylimino groups are oxidized and are further bound with SO_4^{2-} (step 3). Step 4 is the opposite redox process of step 3. Therefore, the PTD-1 shows a hybrid charge-storage mechanism of n/p-type at a low potential (steps 1 and 2) and p-type at a high potential (steps 3 and 4), endowing a high capacity and a high maximum voltage for the Zn//PTD-1 battery.

2.5. Organic Materials as Anodes

According to the electrode potential in an APB, a higher potential electrode is the cathode, while a lower potential electrode is the anode. Therefore, organic materials can be used as cathode or anode, depending on the choice of electrode materials matched. Recently, inspired by the fascinating H^+-storage chemistry, a variety of inorganic and organic materials have been developed to store protons. Especially during the past few years, many research achievements in the inorganic type electrode materials (RuO_2,[91] MnO_2,[92] MoO_3,[93] MXene,[94] and Prussian blue analogues (PBAs)[95]) have surged for storing protons in strong or mildly acidic electrolytes. The inorganic type electrode materials mainly depended on the insertion/extraction process, where the proton is intercalated into the crystal lattice of host materials, showing a good electrochemical performance. Among all the inorganic type electrode materials, the Mn-based materials and PBAs have also attracted increasing attention as cathode materials in APBs for their high reaction potential and capacity (**Figure 4**a).[96] Moreover, based on the deposition/dissolution mechanism (Mn^{2+}/MnO_2 solid–liquid state reaction), the MnO_2 cathode can possess a high cathodic potential (1.229 V vs standard hydrogen electrode (SHE)) and a high theoretical capacity (616 mAh g^{-1}),[97] rendering it a promising cathode material for APBs.

In addition, the development of suitable anode materials for APBs is still a challenge due to the propensity of the

© 2023 The Authors. Advanced Materials published by Wiley-VCH GmbH

15214095, 2023, 42, Downloaded from https://onlinelibrary.wiley.com/doi/10.1002/adma.202302199 by Dalian Institute Of Chemical, Wiley Online Library on [24/01/2024]. See the Terms and Conditions (https://onlinelibrary.wiley.com/terms-and-conditions) on Wiley Online Library for rules of use; OA articles are governed by the applicable Creative Commons License

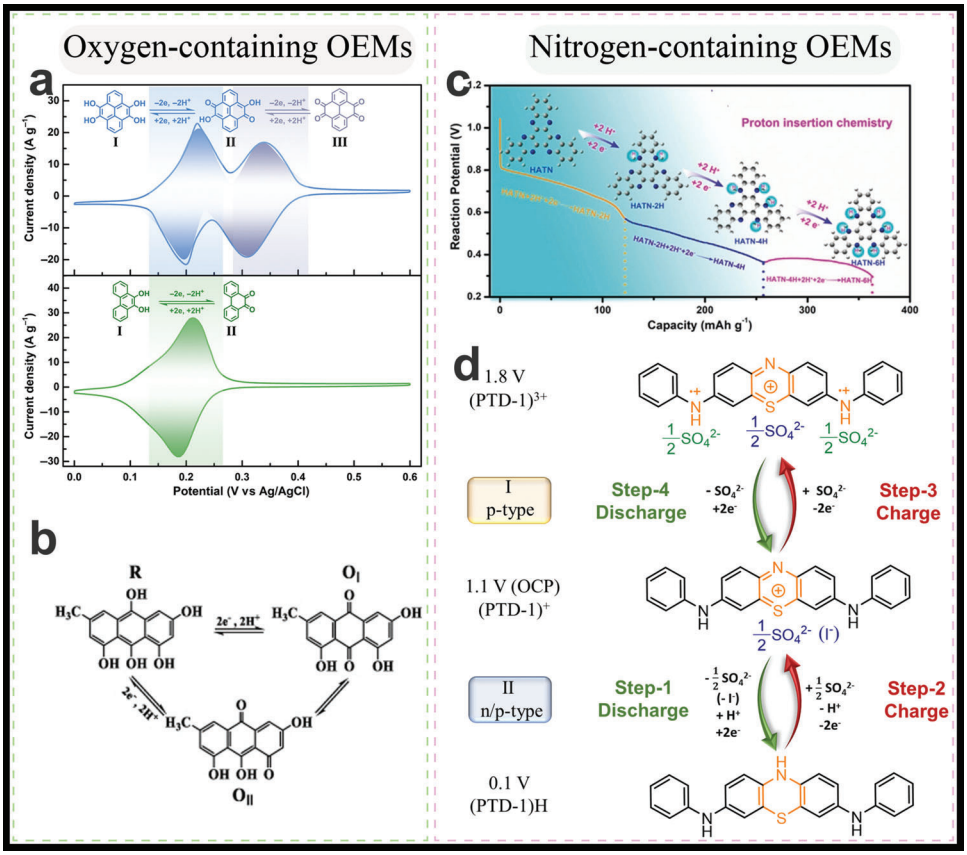

Figure 3. Proton-storage mechanism in oxygen-containing and nitrogen-containing OEMs. a) The proton-storage mechanism and CV curves of PYT/PTO and PQ. Reproduced with permission.[87] Copyright 2020, Chinese Chemical Society. This figure has been published in CCS Chemistry [2021]; [Skeleton Engineering of Isostructural 2D Covalent Organic Frameworks: Orthoquinone Redox-Active Sites Enhanced Energy Storage] is available online at [https://doi.org/10.31635/ccschem.020.202000257; https://www.chinesechemsoc.org/doi/10.31635/ccschem.020.202000257]. b) Emodin molecules. Reproduced with permission.[88] Copyright 2021, Elsevier B.V. c) Structural evolution and protonation pathway during the discharge process of diquinoxalino[2,3-a:2′,3′-c]phenazine (HATN). Reproduced with permission.[89] Copyright 2020, Wiley-VCH. d) Proton-storage mechanism of bis(phenylamino)phenothiazin-5-ium iodide (PTD-1). Reproduced with permission.[90] Copyright 2021, Wiley-VCH.

hydrogen evolution reaction (HER). Because HER can not only change with pH but also can lead to safety concerns due to gas evolution. Organic materials, with the characteristic of reversible proton storage, can be served as cathode or anode, depending on the selection of the other electrode material. To date, quinone-based compounds, with multi-carbonyl redox centers, have attracted much attention for proton insertion. Especially, PTO/PYT, as a typical redox-active molecule, potentially delivers a high output capacity for Li^+ and Zn^{2+} storage.[48,98] Wang's proved that the PTO can be used as a solid-state proton buffer in a 0.5 M H_2SO_4 solution, attributed to the highly reversible enolization reaction of the PTO.[74] Subsequently, the same group proposed a novel hydronium-ion battery (Figure 4b) in a hybrid electrolyte (2 M $MnSO_4$ +2 M H_2SO_4), employing PTO and MnO_2@graphite felt (GF) as the anode and the cathode, respectively.[49] During the charging/discharging process, the cathode showed a reversible Mn^{2+}/MnO_2 deposition/dissolution behavior on the GF and the anode demonstrated a reversible quinone/hydroquinone redox reaction of the PTO with H_3O^+ as the charge carrier. The overall charge-storage mechanism can be explained using the following reaction mechanism.

$$Mn^{2+} + 6H_2O \rightleftharpoons MnO_2 + 4H_3O^+ + 2e^- \quad (3)$$

$$PTO + 2e^- + 2H_3O^+ \rightleftharpoons PTO - 2H + 2H_2O \quad (4)$$

The typical three-electrode measurement was first used to investigate the electrochemical performance of the anode and the cathode. The CV curves show that the PTO anode possesses two pairs of symmetric peaks (Figure 4c). Meanwhile, the PTO anode delivers a high specific capacity of 208 mAh g^{-1} at 0.16 mA cm^{-2}. Figure 4d shows the ex situ FT-IR spectra of the PTO anode during the discharging/charging process in a three-electrode system with (2 M $MnSO_4$ + 2 M H_2SO_4) solution as the electrolyte, where the characteristic absorption peak at ≈1670 cm^{-1} corresponds to the redox-active carbonyl groups of the PTO molecule. Meanwhile, the absorption peak intensity correlates to the content of redox-active carbonyl groups of the PTO molecule. Obviously, the peak intensity of the carbonyl groups decreases and then

 © 2023 The Authors. Advanced Materials published by Wiley-VCH GmbH

15214095, 2023, 42, Downloaded from https://onlinelibrary.wiley.com/doi/10.1002/adma.202302199 by Dalian Institute Of Chemical, Wiley Online Library on [24/01/2024]. See the Terms and Conditions (https://onlinelibrary.wiley.com/terms-and-conditions) on Wiley Online Library for rules of use; OA articles are governed by the applicable Creative Commons License

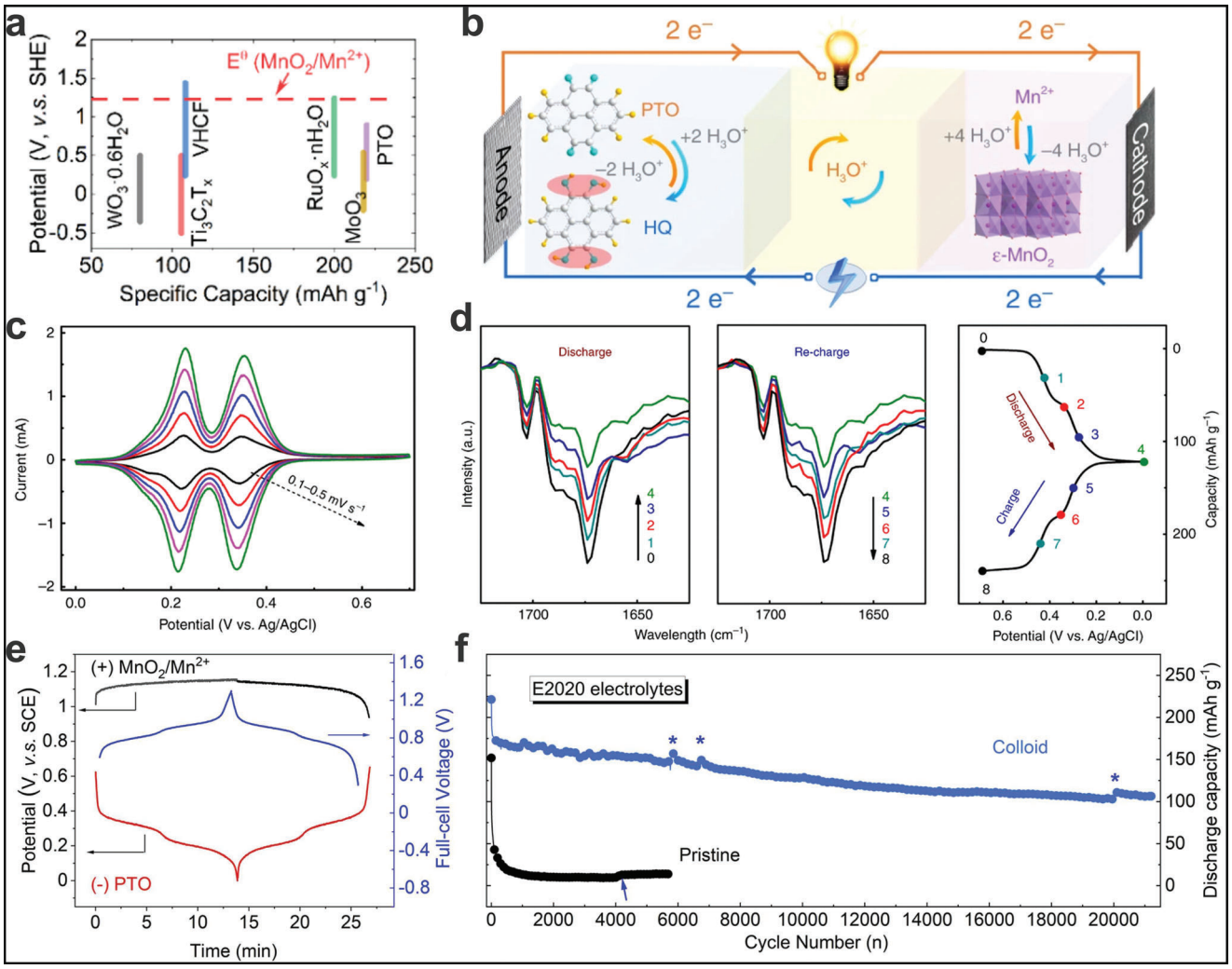

Figure 4. a) A comparison of the reaction potentials and specific capacities for different proton electrodes. Reproduced with permission.[96] Copyright 2022, Elsevier B.V. b) Schematic illustration of the as-assembled PTO//MnO_2@GF proton battery. c) The CV curves at various scan rates, and d) the ex situ FT-IR spectra of the PTO anode. b–d) Reproduced under the terms of the CC-BY Creative Commons Attribution 4.0 International license (https://creativecommons.org/licenses/by/4.0).[49] Copyright 2020, The Authors, published by Springer Nature. e) GCD curves, and f) cycling performances in E2020 electrolytes (2 M H_2SO_4 + 2 M $MnSO_4$). e,f) Reproduced with permission.[96] Copyright 2022, Elsevier B.V.

returns to the original state, during the discharge and recharge processes, further confirming the reversible quinone/hydroquinone redox reaction of the PTO. Moreover, the vibration of the carbonyl groups always exists even in the fully reduced state, demonstrating that carbonyl groups cannot be exhausted from the H_3O^+ storage. The as-fabricated PTO//MnO_2@GF prototype battery delivers a high capacity of 210 mAh g^{-1} at 0.16 mA cm^{-2} (based on the mass loading of the PTO anode), and even at a high current density of 400 mA cm^{-2}, the hydronium-ion battery can maintain a reversible capacity of 66 mAh g^{-1}. Compared with other proton-based batteries/capacitors, the PTO//MnO_2@GF hydronium-ion battery shows a relatively high energy density of 132.6 Wh kg^{-1} at a power density of 25.6 W kg^{-1}, which is calculated based on the mass loading of the PTO and the deposited (or dissolved) MnO_2 during cycling. Interestingly, the PTO//MnO_2@GF battery delivers a specific capacity of 134 mAh g^{-1} at 0.4 mA cm^{-2} at −40 °C, and even at −70 °C, the battery still shows a specific capacity of 110 mAh g^{-1} at 0.4 mA cm^{-2}. Here, due to the presence of protons, the freezing point of the (2 M $MnSO_4$ + 2 M H_2SO_4) electrolyte reduces to approximately −41.6°C, but the diffusion coefficient of Mn^{2+} still cannot be calculated in the mixed electrolyte, due to the fact that proton, Mn^{2+}, and SO_4^{2-} are all potentially involved in the electrochemical energy-storage processes. Moreover, the charge-transfer process is more complicated in a frozen state. Therefore, more attention should be paid to ion diffusion in frozen electrolytes in the future. Later, Zhao's group demonstrated that the MnO_2/Mn^{2+} electrolysis reaction can generate homogeneous and stable colloids in H_2SO_4 (≥1.0 M).[96] These colloidal particles are mainly composed of solid core (MnO_2 nuclei) and the adsorbed sulfate anions, protons, manganese cations, and their hydrated forms, resulting in a lot of water molecules being confined around the colloidal particles. Furthermore, the limited amount of free

 © 2023 The Authors. Advanced Materials published by Wiley-VCH GmbH

15214095, 2023, 42, Downloaded from https://onlinelibrary.wiley.com/doi/10.1002/adma.202302199 by Dalian Institute Of Chemical, Wiley Online Library on [24/01/2024]. See the Terms and Conditions (https://onlinelibrary.wiley.com/terms-and-conditions) on Wiley Online Library for rules of use; OA articles are governed by the applicable Creative Commons License

water is beneficial for enhancing the stability of the anode, resulting in a prolonged cycling life for APBs. As shown in Figure 4e,f, the PTO//MnO_2@GF proton batteries can remain operational for more than 20 000 cycles at 0.5 A g^{-1} in a colloid electrolyte (E2020, 2 M H_2SO_4 + 2 M $MnSO_4$), confirming the colloid-in-acid electrolyte can improve the cycling life and can guarantee excellent reversibility of the PTO//MnO_2@GF battery system. Actually, some electrode materials show poor cycling stability in traditional acid electrolytes, for the co-intercalation of free water molecules. Therefore, reducing the amount of free water in electrolytes may be an effective means to increase the cycling stability of APBs. Interestingly, with the introduction of surfactants such as poly(ethylene glycol) (PEG), the amount of free water decreases due to the formation of hydrogen bonds between water and the PEG molecules, leading to the suppression of the co-intercalation of free water molecules.[99] The resulting full-cell proton battery (VHCF//MoO_3) delivers high stability up to 2000 cycles (77.4% capacity retention) in a PEG-containing 4.2 M H_2SO_4 electrolyte. This strategy also provides an opportunity to improve the cycling stability of APBs using organic materials as electrodes.

Despite PTO proving its worth as an excellent anode for proton storage, it is still not very clear how proton intercalation occurs at the electrode-electrolyte interface. Zhao's group[100] used ex situ thermogravimetric analysis (TGA) and electrochemical quartz crystal microbalance measurements to record the mass changes of the PTO electrode during the charging/discharging process. The large-scale mass changes for the PTO electrode indicate that H_2O molecules and protons get into the lattice of the PTO together, where the charges of protons can be effectively shielded for the existence of H_2O molecules. When the H_2O molecules and protons co-insert into the PTO lattice, the PTO electrode shows a relatively low interfacial resistance at the electrolyte-electrode interface due to the low Coulombic repulsion. Therefore, the PTO electrode shows an excellent electrochemical performance using a three-electrode system in a 4.2 M H_2SO_4 electrolyte, showing a high specific capacity of 376 mAh g^{-1} at 0.05 A g^{-1} (0.25 C, defining 1 C = 0.2 A g^{-1}). It is noteworthy that the PTO electrode exhibits an impressive discharge time of only 7 s at 50 A g^{-1} (250 C), and its capacity recovers remarkably well as the current density decreases, indicating excellent rate performance. Meanwhile, the PTO-based full cell with $K_{0.2}VO_{0.6}[Fe(CN)_6]_{0.8}\cdot 4.1H_2O$ (VHCF) as the cathode, delivers a high capacity of 85 mAh g^{-1} (based on total mass), and an outstanding power density (>10^4 W kg^{-1}) comparable with supercapacitors. An in-depth insight into the proton-storage chemistry at the electrolyte-electrode interface is vital for the development of ultrafast APBs.

The successful application of PTO has stimulated researchers to develop more quinone-based compounds as the anode for APBs. Meanwhile, it is very important to unveil the charge-storage mechanisms of quinone-based compounds during the redox processes. For example, Chen's group designed three different quinones, including benzoquinone (BQ) and its derivatives for APBs.[57] Firstly, for the three quinone-based compounds, the CV measurements were conducted in a three-electrode system with a 0.5 M H_2SO_4 solution as the electrolyte, to evaluate the redox potentials. As shown in **Figure 5**a, the TMBQ shows the lowest reduction potential, attributed to the electron-donating effect of the methyl groups. The TMBQ exhibits a higher LUMO energy, further confirming its lower reduction potential (Figure 5b). In addition, the TMBQ-based device shows a high capacity of 300 mAh g^{-1} at 0.326 A g^{-1} (1 C = 326 mA g^{-1}). The APB was assembled in a mixture of (0.5 M H_2SO_4 + 1 M $MnSO_4$) electrolyte with the TMBQ as the anode, and commercially available GF modified with carbon nanotubes (HGF/CNTs) as the cathode (Figure 5c). The proton battery delivers a reversible capacity of 320 mAh g^{-1} at 0.326 A g^{-1} (1 C) and even at 32.6 A g^{-1} (100 C), the proton battery still delivers a high capacity of 148 mAh g^{-1} (Figure 5d). As shown in Figure 5e, compared with the reported aqueous batteries, the TMBQ//MnO_2 aqueous hybrid battery shows a higher power and energy density. Furthermore, the as-assembled TMBQ//MnO_2 aqueous hybrid battery delivers a capacitance retention of 77% after 4000 cycles (Figure 5f). This work demonstrates the proton storage and transport mechanism in quinone-based electrodes and provides a promising direction for high-performance APBs.

2,6-Dihydroxyanthraquinone (DHAQ), as a typical redox-active anthraquinone (AQ)-based molecule, delivers a specific capacity of 110 mAh g^{-1} in 1 M H_2SO_4.[101] The APB was assembled employing DHAQ as the anode, a piece of carbon felt as the cathode, and (0.5 M $MnSO_4$ + 1 M H_2SO_4) as the electrolyte, showing a discharge capacity of around 90 mAh g^{-1} at 1.13 A g^{-1}. The DHAQ//carbon felt APB demonstrates a non-ideal electrochemical behavior due to the limited capacity of the DHAQ. Therefore, rational design and fabrication of organic electrodes are of great importance for improving the overall electrochemical performance of APBs. Besides, it has been proven that ALO-based anode also exhibits a reversible storage of H^+, which can be matched well with the carbon felt-based cathode accompanied by the Mn^{2+}/MnO_2 conversion reaction.[58] Besides, the H_2SO_4 and $MnSO_4$ mixed solution is replaced with (2 M HBF_4 + 2 M $Mn(BF_4)_2$), endowing the electrolyte with a low freezing point (−160 °C). Accordingly, the ALO//CF proton batteries achieve a discharge capacity of 85 mA h g^{-1} at −90 °C.

π-Conjugated N-containing organic compounds, with rich C=N moieties as active sites, have attracted much attention for energy storage due to their high theoretical capacity.[102] Here, diquinoxalino [2,3-a:2′,3′-c] phenazine (HATN) with six C=N moieties, was designed to assure the capability of H^+ storage. The HATN//β-MnO_2 proton battery shows a high specific capacity of 260 mAh g^{-1} at 0.1 A g^{-1}, which can be attributed to the abundant N active centers and the π-conjugated structure of the HATN anode.[103] In another example, Xu's group reported a new APB, where the phenazine derivative (dipyridophenazine [DPPZ]) was used as the anode, and indium hexacyanoferrate (InHCF) was employed as the cathode.[104] The DPPZ is *N*-heterocyclic and a redox-active molecule, showing a low potential and a high theoretical specific capacity. PBAs show a reversible intercalation/deintercalation of H^+ and a high output potential, which can be used as a suitable cathode material for APBs. The as-constructed DPPZ//InHCF proton battery delivers a low and reversible specific capacity of 37 mA h g^{-1} at 1 A g^{-1} based on the total mass loading of the active materials of the cathode and the anode, and at 10 A g^{-1}, the proton battery can deliver a capacity of 30.1 mAh g^{-1}. In addition, the DPPZ//InHCF proton battery shows an energy density of ≈28 Wh kg^{-1}. In order to design a binder-free and flexible electrode for APBs, Yan's group integrated a redox-active polymer (PDPZ) with titanium

© 2023 The Authors. Advanced Materials published by Wiley-VCH GmbH

15214095, 2023, 42, Downloaded from https://onlinelibrary.wiley.com/doi/10.1002/adma.202302199 by Dalian Institute Of Chemical, Wiley Online Library on [24/01/2024]. See the Terms and Conditions (https://onlinelibrary.wiley.com/terms-and-conditions) on Wiley Online Library for rules of use; OA articles are governed by the applicable Creative Commons License

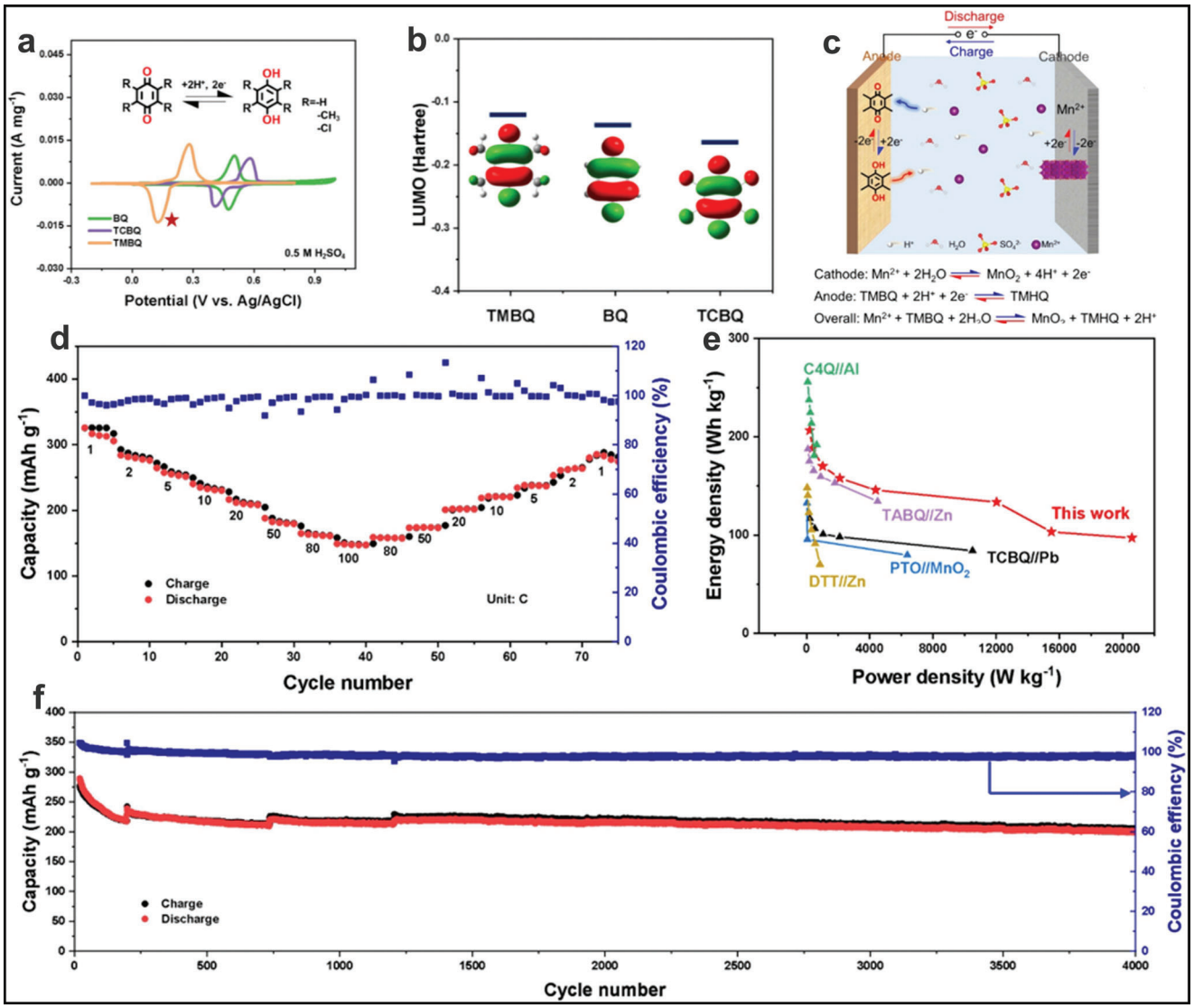

Figure 5. a,b) Comparison of the CV curves at 1 mV s^{-1} (a) and the LUMO energy levels (b) of benzoquinone (BQ) and its derivatives. c) Schematic illustration of the as-assembled TMBQ//MnO_2 aqueous hybrid battery. d) Rate performance, e) Ragone plot, and f) cycling performance at 5 C of the TMBQ//MnO_2 hybrid battery. a–e) Reproduced with permission.[57] Copyright 2022, Wiley-VCH.

carbide ($Ti_3C_2T_x$) MXene via a facile vacuum-assisted filtration approach,[54] where the PDPZ polymer is comprised of PDPZ structural unit (**Figure 6**a). As shown in the SEM and TEM images of the PDPZ@MXene composites (Figure 6b,c), the PDPZ nanoparticles are embedded into the 3D laminated architecture of the MXene, which can facilitate the electron transfer and lead to a fast redox reaction. The in situ FTIR measurements confirm the reversible proton uptake reaction between the C=N and the C–N/N–H bonds in the PDPZ molecules (Figure 6d). To investigate the practical applications of binder-free electrodes in portable and wearable electronic devices, a quasi-solid and flexible APB was constructed using PDPZ@MXene as the anode, CuFePBA@MXene as the cathode, and poly(vinyl alcohol) (PVA)-H_2SO_4 gel as the electrolyte, delivering a high specific capacity of 74.5 mAh cm^{-3} at 1 A cm^{-3} based on the entire device volume. Moreover, the flexible APB can reach a maximum power density of 6000 mW cm^{-3}. Interestingly, the as-assembled APB not only works under various bending deformations but also shows excellent capacitance retention of ≈98.2% after 10 000 cycles. Despite the considerable cyclic retention rate demonstrated in the above literature, maintaining high cycle stability can be challenging due to significant water loss during the cycling process for flexible electrolytes (such as polyacrylamide and PVA, among others). Flexible electrolytes without polymers, such as "water-in-salt" electrolytes, can provide a higher water retention ability, increase the electrochemical window of devices, and reduce the dissolution of electrode materials.[105] Thus, the development of a "water-in-salt" electrolyte system is still needed to meet the requirements for portable and wearable APBs.[106]

To increase the cycling performance, a feasible approach is the polymerization of organic compounds, which is expected to show a suppressed solubility in electrolytes and a fast electron

 © 2023 The Authors. Advanced Materials published by Wiley-VCH GmbH

15214095, 2023, 42, Downloaded from https://onlinelibrary.wiley.com/doi/10.1002/adma.202302199 by Dalian Institute Of Chemical, Wiley Online Library on [24/01/2024]. See the Terms and Conditions (https://onlinelibrary.wiley.com/terms-and-conditions) on Wiley Online Library for rules of use; OA articles are governed by the applicable Creative Commons License

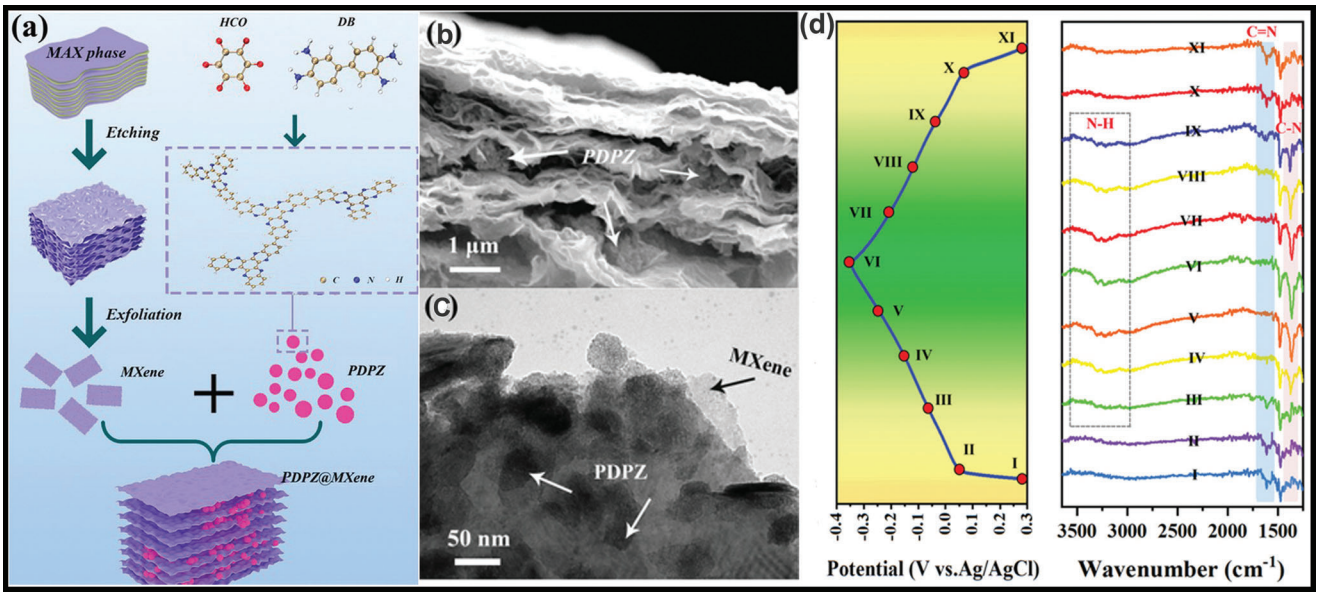

Figure 6. a) The preparation of the PDPZ@MXene composite. b) SEM image and c) TEM image of the PDPZ@MXene composites. d) In situ FT-IR investigation on the PDPZ@MXene electrode. a–d) Reproduced with permission.[54] Copyright 2022, Wiley-VCH.

transfer.[107] For example, Tao's group constructed an APB using polyaniline (PANI) as the anode, carbon felt as the cathode, and 3.5 M $Mn(ClO_4)_2$ as the electrolyte.[108] The APB delivers a discharge capacity of 85 mA h g^{-1} based on the mass of PANI at a high current density of 18 A g^{-1}, showing an excellent rate performance. In addition, the APB exhibits capacity retention of 82% after 500 cycles. The $Mn(ClO_4)_2$ electrolyte can reduce the freezing point to −122 °C, endowing a discharge capacity of 112 and 52.9 mAh g^{-1} at −50 and −70 °C, respectively, for the APB. Furthermore, PANI can be introduced into the MoO_3 electrode to improve electrical conductivity and cycling stability.[109] The PANI-MoO_3 nanobelt electrode delivers a higher specific capacity of 236.1 mAh g^{-1} at 1 A g^{-1} and excellent capacitance retention of 95.5% after 6000 cycles using a three-electrode system in a 1 M H_2SO_4 electrolyte, which can be attributed to the synergistic effect between the PANI and the MoO_3. Here, the proton battery–supercapacitor hybrid device was assembled with the PANI–MoO_3 as the anode and nitrogen-doped activated carbon as the cathode, showing a maximum energy density of 43.3 Wh kg^{-1} at a power density of 800 kW kg^{-1}. In addition, polyimide (PI) was also designed using 1,4,5,8-naphthalenetetracarboxylic dianhydride (NTCDA) and urea, which can be used as the anode to match with the MnO_2@GF cathode.[110] The PI//MnO_2@GF device delivers capacitance retention of 67.9% at 5 A g^{-1} after 5000 cycles.

2.6. Organic Materials as Cathodes

It is highly desirable to use organic materials with a high capacity and a high redox potential (a low LUMO energy) as cathode materials in full APBs because cathode materials often determine the energy density which depends on the voltage window. To further extend the voltage window, the selection of suitable anode materials with a low redox potential, can lead to an improvement of the energy density. In general, a metal (such as Pb) is selected as the anode for its relatively low redox potential (−0.36 V vs SHE), high structural stability, and excellent energy-storage capability in the H_2SO_4 electrolyte.[111] Niu's group used p-chloranil (PCHL) as the cathode to assemble an aqueous Pb//quinone battery (**Figure 7**a), demonstrating the H^+ insertion chemistry in an anti-freezing electrolyte (5 M H_2SO_4).[112] The porous rGO foam was introduced to further improve the electrical conductivity and stability of the hybrid cathode. In general, the freezing of water is due to the formation of hydrogen bonds between water molecules.[113] However, as shown in Figure 7b, the SO_4^{2-} in the anti-freezing electrolyte can interact with water molecules via hydrogen bonding, leading to the breaking of the hydrogen bonds between the water molecules, which can not only reduce the freezing point of aqueous electrolytes but also can provide a high ionic conductivity even at −70 °C. To ensure the potential matching between the PCHL cathode and the Pb anode, the individual electrode was measured using a three-electrode system with a 5 M H_2SO_4 as the electrolyte. Obviously, the PCHL cathode shows a high output potential (Figure 7c) and the calculated LUMO energy (−4.35 eV) of PCHL is lower than most of the organic materials, further demonstrating its high reduction potential. The CV and GCD curves (Figure 7d–f) manifest the kinetic reversibility during the redox reaction and a much larger capacitance of the Pb//PCHL–rGO battery (208 mAh g^{-1} at 0.2 A g^{-1} and a reversible capacity of 84 mAh g^{-1} even at 100 A g^{-1}), which is superior to the reported aqueous battery (Figure 7g). The Pb//PCHL–rGO battery also delivers good cycle stability after 3000 cycles at 10 A g^{-1} (Figure 7h). Moreover, the low-temperature electrochemical performance of the Pb//PCHL-rGO battery was tested in a 5 M H_2SO_4 electrolyte. It shows a discharge capacity of 119 and 87 mAh g^{-1} at a current density of 0.1 A g^{-1} at −40 and −70 °C, respectively, and a long cycle stability at extremely cold conditions (−70 °C). Currently, a highly concentrated acidic solution remains a viable option for

 © 2023 The Authors. Advanced Materials published by Wiley-VCH GmbH

15214095, 2023, 42, Downloaded from https://onlinelibrary.wiley.com/doi/10.1002/adma.202302199 by Dalian Institute Of Chemical, Wiley Online Library on [24/01/2024]. See the Terms and Conditions (https://onlinelibrary.wiley.com/terms-and-conditions) on Wiley Online Library for rules of use; OA articles are governed by the applicable Creative Commons License

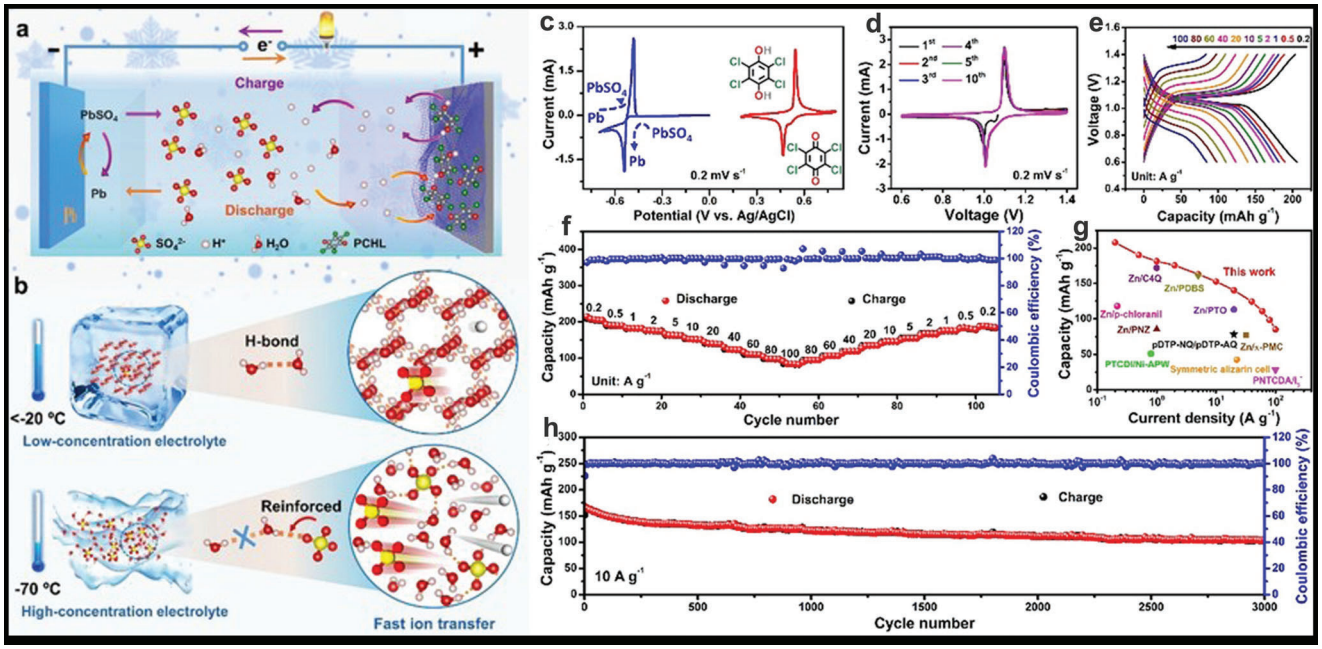

Figure 7. a) Schematic illustration of the as-fabricated Pb//PCHL–rGO battery. b) The anti-freezing mechanism for acid electrolytes. c) CV curves of the anode and the cathode materials in a three-electrode system. d) CV curves at 0.2 mV s^{-1}, e) GCD curves, and f) rate capability of the Pb//PCHL-rGO battery. g) A comparison of the capacity with other aqueous batteries. h) Cycling performance. a–h) Reproduced with permission.[112] Copyright 2021, Wiley-VCH.

low-temperature electrolytes in APBs. Additionally, due to the fast reaction kinetics of the H^+ insertion chemistry, this work represents a new opportunity to construct APBs working at low temperatures.

Later on, as shown in **Figure 8**a, PTO/PYT with a fast kinetics of H^+ uptake/removal and a reasonable reduction potential (0.5 V vs SHE) was matched with the Pb anode in an acidic electrolyte (1 M H_2SO_4), where the discharged PTO cathode can be further oxidized by the dissolved oxygen via H^+ extraction.[114] Interestingly, the cathode of the discharged PTO and oxygen from air show a large potential difference, as oxygen has a higher standard electrode potential in an aqueous acidic medium than in a neutral medium, leading to a spontaneous redox reaction. Therefore, the Pb//PTO battery can not only show an excellent electrochemical performance for the fast reaction kinetics via H^+ insertion chemistry but also exhibits enhanced air-rechargeability. The CV curves of the Pb//PTO battery show two pairs of distinctly reversible redox peaks (Figure 8b), which can be attributed to the reversible two-step redox reactions during the charge/discharge process. In addition, as shown in Figure 8c, the resulting Pb//PTO battery exhibits a high specific capacity of 229 mAh g^{-1} at 0.2 A g^{-1} and a reversible capacity of 77 mAh g^{-1} even at a high current density of 120 A g^{-1}. After repeated self-charging/galvanostatic discharging, the Pb//PTO battery also delivers a capacity retention of 68% at 1 A g^{-1}. The exciting results stimulate researchers to develop aqueous self-powered systems with long cycle life.

Apart from those carbonyl-containing organic materials, organic electrodes with nitrogen as the active center have been developed to serve as the cathode owing to the easy and controlled synthesis of the nitrogen-containing organic compounds.[115] Lu's group presented a 2,5-dichloro-1,4-phenylene bis((ethylsulfonyl)amide) (HDC) cathode with nitrogen as the active center (Figure 7d),[76] showing a higher working potential (≈1.0 V vs SHE) than the reported cathodes, such as tetrachloro-1,4-benzoquinone (TCBQ) (0.91 V vs SHE) and PTO (0.51 V vs SHE).[116] Besides, the HDC possesses a high theoretical capacity of 148 mAh g^{-1}, highlighting it as a potentially novel cathode material. Meanwhile, the cost-effective quasi-solid electrolyte (QSE) was also designed to further improve the potential window and the mechanical properties. The HDC//activated carbon (AC) full cell was fabricated by sandwiching HDC cathode, QSE, and AC anode, showing a discharge capacity of 50 mAh g^{-1} at a current density of 0.1 A g^{-1} (32 mAh g^{-1} at 1 A g^{-1}), coupling with stable cycle performance (showing capacity retention of 89.7% over 2000 cycles at 1 A g^{-1}). Later, a metal-free quasi-solid flexible battery was fabricated to further evaluate the electrochemical performance of the HDC (Figure 7e). The results show that the assembled battery exhibits good cycling stability (Figure 7f), high Coulombic efficiency, and excellent flexibility. This work provides a strategy to improve the output potential of cathode materials in H^+-storage chemistry via grafting with electron-withdrawing atoms (–F, –Cl, –I) or groups (–SO_2–). In addition, more stable and electrode-compatible quasi-solid electrolytes need to be developed to further widen the working window of the electrolyte.

2.7. Organic Materials as both Anodes and Cathodes

To date, all-organic batteries employing organic materials as both the anode and the cathode have emerged as promising

© 2023 The Authors. Advanced Materials published by Wiley-VCH GmbH

15214095, 2023, 42, Downloaded from https://onlinelibrary.wiley.com/doi/10.1002/adma.202302199 by Dalian Institute Of Chemical, Wiley Online Library on [24/01/2024]. See the Terms and Conditions (https://onlinelibrary.wiley.com/terms-and-conditions) on Wiley Online Library for rules of use; OA articles are governed by the applicable Creative Commons License

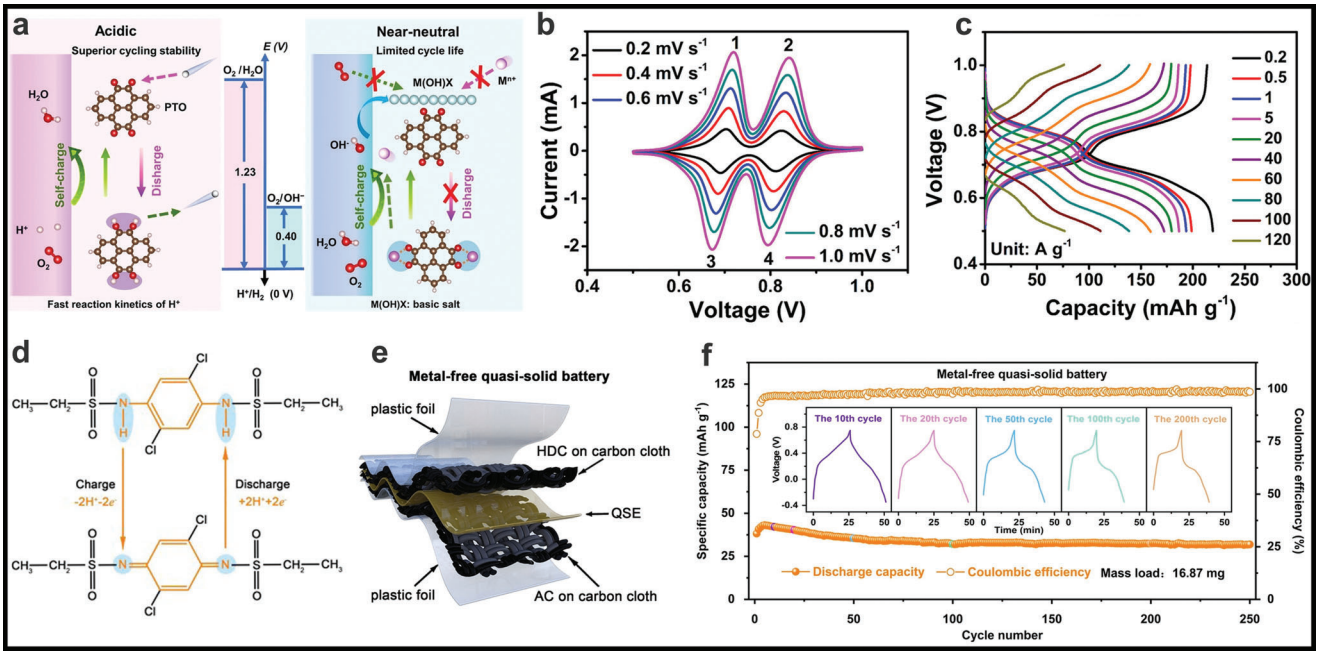

Figure 8. a) Schematic illustration of the self-charging Pb//PTO battery. b) CV curves at different scan rates, and c) GCD curves of the Pb//PTO battery. a–c) Reproduced with permission.[114] Copyright 2022, Wiley-VCH. d) Energy-storage mechanism of the HDC. e) Illustrations of the HDC//AC full quasi-solid flexible device, and f) the corresponding cycling performance at 0.1 A g^{-1}. d–f) Reproduced with permission.[76] Copyright 2022, Wiley-VCH.

energy-storage units based on metal-ion electrolytes containing Li^+ or Na^+ due to the merits of sustainability and environmental friendliness.[117,118] However, these all-organic batteries based on metal-ion electrolytes still suffer from some drawbacks, such as the sluggish ion-transport and safety concerns of metal ions. Fortunately, due to the fascinating proton chemistry, all-organic batteries consisting of both redox-active molecules are designed to further boost the flourishing of metal-free APBs. As early as 2017, Sjödin's group successfully assembled an all-organic proton battery in a proton donor and acceptor slurry consisting of 2-fluoropyridinium triflate and 2-fluoropyridine (**Figure 9**a), where the AQ and benzoquinone (BQ) functionalized poly(3,4-ethylenedioxythiophene) (PEDOT) were used as the anode and the cathode, respectively.[75] Even without any conducting additives in the materials, the PEDOT, as the conducting polymer backbone, can ensure rapid electron transport. Simultaneously, the PEDOT can suppress the dissolution of redox moieties into the electrolyte. The conducting polymer of PEDOT-AQ and PEDOT-BQ with the quinone/hydroquinone (Q/QH_2) redox couple, exhibits a reasonable potential difference in the three-electrode voltammogram (Figure 9b). To investigate the effect of PEDOT-AQ or PEDOT-BQ (Figure 9c) for the two-electrode battery, the cells were assembled with an n/p ratio of approximately 1:2 (negative limiting) or 2:1 (positive limiting). The resulting all-organic proton battery possesses a specific capacity of 103 and 120 mAh g^{-1} via using PEDOT-AQ and PEDOT-BQ as the limiting material, respectively, further verifying the feasibility of all-organic APBs.

Inspired by the aforementioned promising results, Sjödin's group further designed thiophene-based trimeric structures, functionalized with naphthoquinone (NQ) or hydroquinone (QH_2) pendent groups.[119] As shown in Figure 9d, the pendants were used as charge carriers for protons showing a reversible redox reaction with a two-electron-transfer process, which determines the electrochemical performance of the APB. Firstly, the so-called post-deposition polymerization method was adopted to prepare polymers, with the terthiophene trimer (Figure 9e) as precursors. Typically, the trimeric structures were deposited as a layer onto the conductive substrate, by drop-casting the trimer solution and by removing the solvent under vacuum. The deposited trimer was further polymerized to form conducting polymers by applying a voltage (0.81 V vs SHE) in a 0.5 M sulfuric solution. This method of polymerization is named post-deposition polymerization, demonstrating the numerous advantages such as easy processing, high material utilization, and high electron conductivity, without the need for conductive additives and binders. Once the post-deposition polymerization was demonstrated to be feasible, the QH_2 and NQ as the pendant groups were attached to the 3,4-propylenedioxythiophene to form two new trimers, named as EP(QH_2)E and EP(NQ)E, respectively (Figure 9f). These trimers were further polymerized to form the redox-active conducting polymers, which can be employed as the anode (pEP(NQ)E) and the cathode (pEP(QH_2)E) to assemble novel APBs in acid electrolytes. A 3.3 M H_2SO_4 electrolyte was used to investigate the electrochemical performance of the APB at a low temperature (−24 °C). The assembled battery delivers a specific capacity of 60 mAh g^{-1} coupled with an average cell voltage of 0.4 V. The authors proposed a strategy to further improve the capacity by optimizing the linkage or by increasing the number of redox groups. In 2021, the same group used quinizarin (Qz) to prepare conducting polymers using a similar method.[120] Here, the naphthoquinone (NQ) and quinizarin (Qz) based conducting polymers served as the anode and the cathode, respectively, for the APB in a protic ionic liquid electrolyte (Figure 9g),

© 2023 The Authors. Advanced Materials published by Wiley-VCH GmbH

15214095, 2023, 42, Downloaded from https://onlinelibrary.wiley.com/doi/10.1002/adma.202302199 by Dalian Institute Of Chemical, Wiley Online Library on [24/01/2024]. See the Terms and Conditions (https://onlinelibrary.wiley.com/terms-and-conditions) on Wiley Online Library for rules of use; OA articles are governed by the applicable Creative Commons License

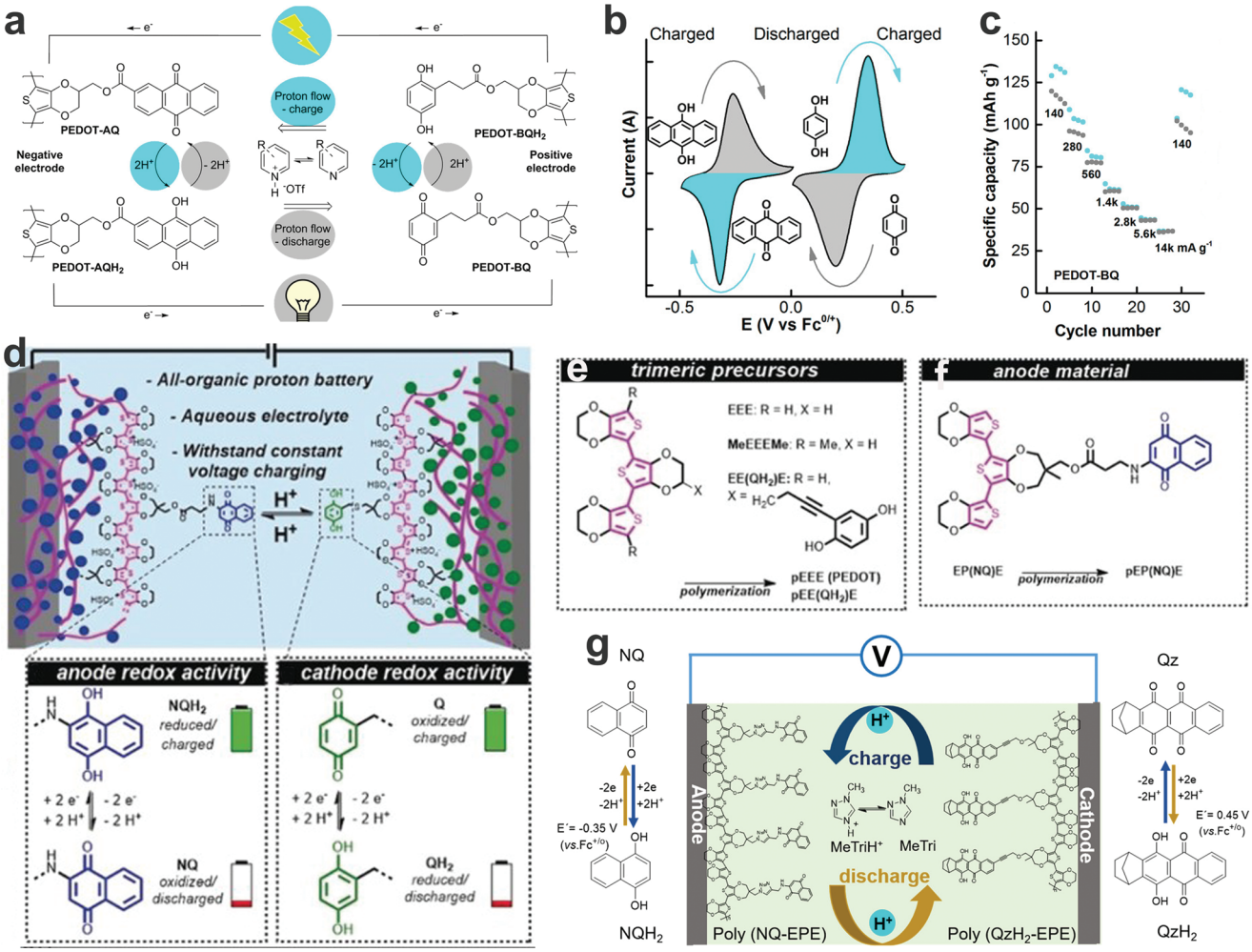

Figure 9. Schematic illustration of all organic APBs. a) The conducting polymer of PEDOT-AQ and PEDOT-BQ served as the anode and the cathode, respectively. b) The CV curves of PEDOT-AQ and PEDOT-BQ in three-electrode, c) Specific capacity of PEDOT-BQ. a–c) Reproduced with permission.[75] Copyright 2017, American Chemical Society. d) The AQ and QH_2 were used as the anode and the cathode of APBs. e) Thiophene-based trimeric precursors for the post-deposition polymerization process. f) The QH_2 as a pendent group was attached to the conducting polymer. d–f) Reproduced with permission.[119] Copyright 2020, The Authors, published by Wiley-VCH. g) PEDOT units functionalized with AQ and BQ were used as the anode and the cathode, respectively. Reproduced under the terms of the CC-BY Creative Commons Attribution 4.0 International license (https://creativecommons.org/licenses/by/4.0).[120] Copyright 2021, The Authors, published by American Chemical Society.

delivering a capacity of 62 mAh g^{-1} and capacity retention of 80% after 500 cycles.

Conducting polymers with the possibility of tailoring electrochemical properties provide more opportunities to improve the performance of APBs. In addition, the donor–acceptor (D–A) conjugated polymers can allow the charge transfer from the donor unit to the acceptor unit within the molecule, resulting in an enhancement of the charge transport. Apart from the mentioned thiophene-based trimeric conducting polymers, Tang's group reported the synthesis of dithieno[3,2-b:2′,3′-d]pyrrole (DTP) twisted quinone based conducting polymers for high-performance all-organic proton battery (**Figure 10**a).[62] The twisted DTP-AQs or DTP-NQs are the redox-active units, which can promote charge transport along the conjugated backbone and facilitate the electrochemical reaction kinetics (Figure 10b). The all-organic proton battery (Figure 10c) was fabricated by employing the NQ-based materials and the AQ-based materials as the anode and the cathode, respectively, due to the large difference in the LUMO energy level between the DTP-AQ (−3.72 eV) and the DTP-NQ (−3.81 eV) (Figure 10d). Meanwhile, the CV curves of the two electrode materials show a significant potential difference (Figure 10e) and high specific capacities (Figure 10f), ensuring the possibility to construct an all-organic proton battery. The as-fabricated proton battery shows a high specific capacity of 78 mAh g^{-1} at 0.5 A g^{-1}, capacity retention of 50% at a high current density of 20 A g^{-1}, and cyclability of 66% after 1000 cycles at 1 A g^{-1} (Figure 10g). The decrease in the specific capacity after long-term cycling is due to the possible degradation of the quinone-based polymers, which requires a further delicate design of their chemical structures.

The advent of new technologies of the "Internet of Things", smart packaging and clothing, and flexible electronic devices, has led to a demand for energy-storage systems that are lightweight, cost-effective, and flexible, while also capable of powering these

 © 2023 The Authors. Advanced Materials published by Wiley-VCH GmbH

15214095, 2023, 42, Downloaded from https://onlinelibrary.wiley.com/doi/10.1002/adma.202302199 by Dalian Institute Of Chemical, Wiley Online Library on [24/01/2024]. See the Terms and Conditions (https://onlinelibrary.wiley.com/terms-and-conditions) on Wiley Online Library for rules of use; OA articles are governed by the applicable Creative Commons License

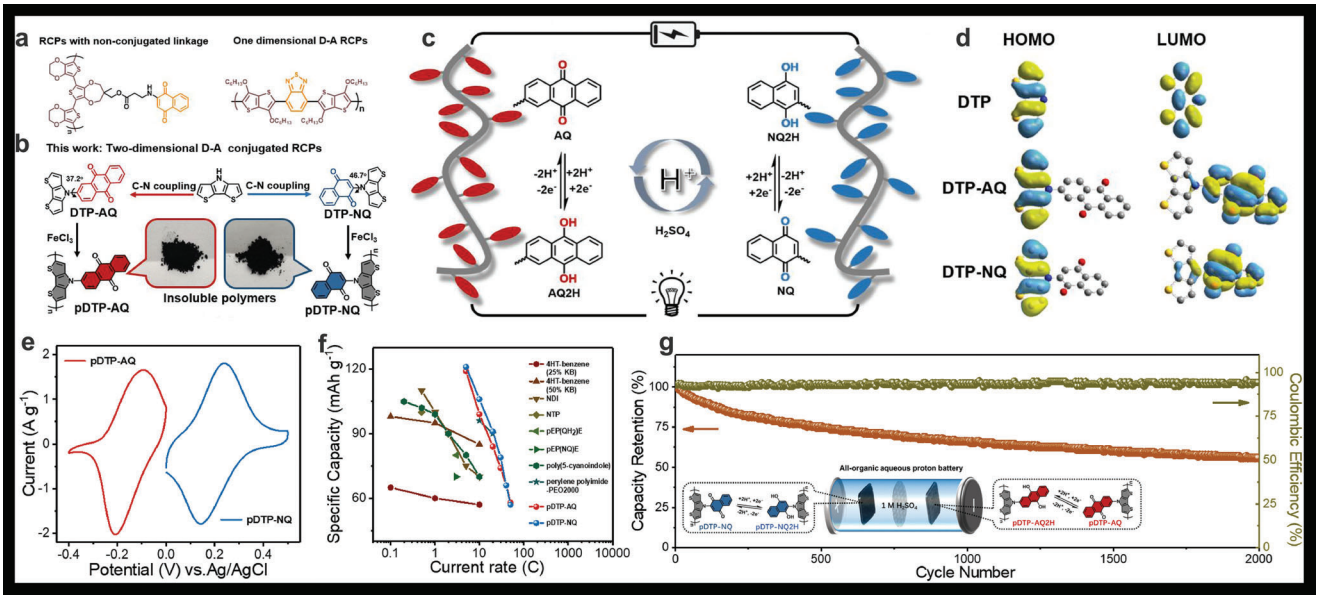

Figure 10. a) Comparison of the poly(terthiophene) based electrode and the D–A conjugated polymer. b) The stepwise design of the dithieno[3,2-b:2′,3′-d]pyrrole (DTP) twisted quinone. c) Schematic illustration of all organic APBs with the anthraquinone or the naphthoquinone as charge carriers. d) The HOMO and LUMO of the as-obtained molecules. e) CV curves of the cathode and the anode materials in a three-electrode system. f) A comparison with organic electrodes in literature. g) The long-term cycling performance of the all-organic APB. a–g) Reproduced with permission.[62] Copyright 2021, Elsevier B.V.

devices. All-polymer batteries are one type of energy-storage system that holds the potential to meet these requirements. Chao's research group designed an all-polymer-based APB, in which the capacitive-type catechol-based polymer, diffusion-type anthraquinone-based polymer, and 0.5 M H_2SO_4 solution served as the anode, the cathode, and the electrolyte, respectively.[121] The as-fabricated proton battery delivers a high specific capacity of 78.1 mAh g^{-1} at 0.5 A g^{-1} accompanied by a voltage plateau (0.3 to 0.9 V). Therefore, the rational design of polymers can significantly enhance the electrochemical performance of APBs. In addition, some organic copolymers (AN-TA and AN-PA) were synthesized, which are composed of different tertiary amines showing reversible proton storage.[122] The assembled proton battery exhibits an enhancement of the electrochemical performance at a sub-zero temperature (−25 °C). The traditional PANI, with a reversible proton insertion/extraction, can be used as the cathode for the APB. The as-constructed diquinoxalino-phenazine (DPZ)//PANI device shows a maximum specific capacity of 61.5 mAh g^{-1} based on the total mass loading of the active materials of the cathode and the anode. Moreover, the assembled hexaazatrinaphthalene (HATN)@MXene//PANI flexible proton battery delivers a specific capacity of 90.1 mAh cm^{-3} based on the volume of the whole device, demonstrating its great potential for practical applications.[55,123]

Apparently, based on the abovementioned research, it is observed that all-organic proton batteries generally include two different molecules with a large difference in the redox peak position between the anode and the cathode, resulting in a more complicated operation process and a high cost. It is necessary to develop a symmetric all-organic proton battery, by using one molecule with two distinct redox couples. Originally, quinone-amine polymers played dual roles as both the cathode and the anode in symmetric all-organic APBs, indicating the high potential of these quinone-amine polymer-based electrode materials for practical applications.[124] Subsequently, Niu's group prepared a π-conjugated poly(2,9-dihydroquinoxalino[2,3-b]phenazine) (PO) molecule, which can be used as the anode and the cathode of symmetric all-organic proton battery in a $ZnSO_4$ electrolyte (**Figure 11**a).[125] The LUMO and HOMO energy levels of the PO and its protonation products (P and PR) are investigated (Figure 11b), where the LUMO energy of PO and PR is −3.62 and −0.41 eV, respectively. Obviously, the large difference in the LUMO energy between PO and PR can result in a high output potential, ensuring the fabrication of the symmetric all-organic proton battery. The CV curve of the Zn/PO half battery shows two redox couples at about 1 and 0.4 V vs Zn/Zn^{2+} (Figure 11c), which is consistent with the above results. Compared with the reported proton battery, the symmetric all-organic proton battery (PO//PO) delivers a high specific capacity of 147 mAh g^{-1} at 0.1 A g^{-1} and excellent rate performance (90 mAh g^{-1} at 2 A g^{-1}), which broadens the applications of organic molecules for proton batteries. However, the proton-storage chemistry of organic electrodes in aqueous electrolytes containing Zn^{2+} is still controversial due to the competitive role between proton and Zn^{2+} during the energy-storage process, which requires more experimental research and theoretical support to unveil the exact energy-storage mechanism.

Furthermore, bipolar electroactive organic molecules, with electron-accepting and electron-donating properties, hold great potential for the symmetric all-organic proton battery. Tao's group designed a bipolar poly(aminoanthraquinone) (PNAQ) via a simple one-step oxidative polymerization reaction.[126] The introduction of the polyaniline-like skeleton can improve the conductivity and stability of the PNAQ. Moreover, the

 © 2023 The Authors. Advanced Materials published by Wiley-VCH GmbH

15214095, 2023, 42, Downloaded from https://onlinelibrary.wiley.com/doi/10.1002/adma.202302199 by Dalian Institute Of Chemical, Wiley Online Library on [24/01/2024]. See the Terms and Conditions (https://onlinelibrary.wiley.com/terms-and-conditions) on Wiley Online Library for rules of use; OA articles are governed by the applicable Creative Commons License

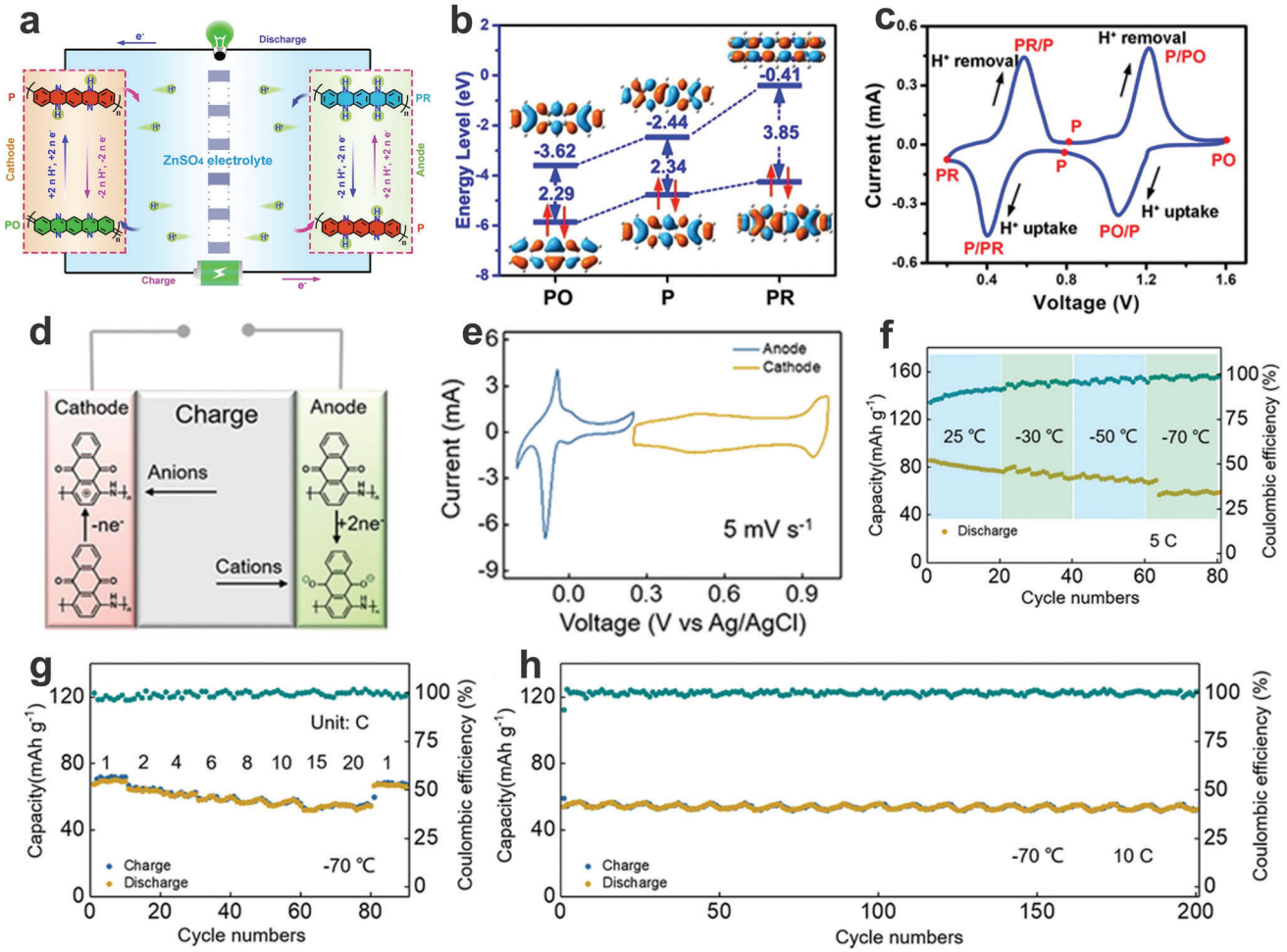

Figure 11. a) Schematic illustration of symmetric all-organic APBs. b) The LUMO and HUMO energy of PO and its protonation products (P and PR). c) CV curve of the Zn//PO half battery. a–c) Reproduced with permission.[125] Copyright 2022, Wiley-VCH. d) The working mechanism of the symmetric battery. e) The CV curves of PNAQ in a 4 M H_2SO_4 electrolyte. f) Discharge capacity at different temperatures. g) Rate performance and h) cycling stability of symmetric battery at −70 °C. d–h) Reproduced with permission.[126] Copyright 2021, Wiley-VCH.

quinone-based moieties (the anode) and the benzene ring-based units (the cathode) of the PNAQ correspond to the H^+ reversible uptake/removal and the adsorption/desorption of HSO_4^- (Figure 11d), respectively. Obviously, the CV curves of the PNAQ show obvious redox peaks in the range of approximately −0.2 to 0.25 V vs Ag/AgCl or ≈0.25–1.0 V vs Ag/AgCl (Figure 11e), confirming the bipolar character of the PNAQ. Finally, the symmetric all-organic proton battery delivers a discharge capacity of 85 and 60.4 mAh g^{-1} at 25 and −70 °C, respectively (Figure 11f). As shown in Figure 11g,h, even at −70 °C, the symmetric all-organic proton battery still shows excellent rate performance (a discharge capacity of 55.1 mAh g^{-1} at 2.4 A g^{-1}) and superior cycling stability. Besides, some bipolar quinone-based small molecules (alizarin) can be used as both the anode and the cathode of the symmetric all-organic proton battery.[127] These encouraging results further broaden the chemistry of all-organic proton batteries. Although finding compatible organic cathode and anode materials poses challenges, the pursuit of replacing metal-based electrodes with organic ones is meaningful as it promises to eliminate metals entirely from batteries, ultimately enabling the development of metal-free batteries (**Table 1**).

3. Conclusion and Outlook

Protons, as the smallest and lightest ions, hold great promise in high-performance energy-storage devices. By carefully choosing appropriate anode and cathode materials, implementing a strategic approach to molecular engineering and organic electrode materials, and fine-tuning electrolytes, APBs have the potential to achieve exceptional operational safety, high energy and power density, and long-term cycling stability. In this review, we have summarized the recent development of organic electrode materials in APBs. Compared with traditional inorganic-type electrode materials such as manganese oxides, vanadium oxides, molybdenum oxides, and PBAs, organic materials have attracted significant attention as advanced materials for APBs due to their structural diversity, rich proton-storage sites, and abundant resources. The low density of organic materials facilitates the fast diffusion and accommodation of ions during charge and

 © 2023 The Authors. Advanced Materials published by Wiley-VCH GmbH

15214095, 2023, 42, Downloaded from https://onlinelibrary.wiley.com/doi/10.1002/adma.202302199 by Dalian Institute Of Chemical, Wiley Online Library on [24/01/2024]. See the Terms and Conditions (https://onlinelibrary.wiley.com/terms-and-conditions) on Wiley Online Library for rules of use; OA articles are governed by the applicable Creative Commons License

Table 1. The comparison of various proton batteries using organic electrodes.

Cathode	Anode	Electrolyte	Out voltage	Capacity	Cycle life (retention)	Energy/power density [Wh kg^{-1}/kW kg^{-1}]	Refs.
Pristine carbon felt	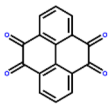	2 м H_2SO_4 + 2 м мnSO$_4$	–	–	21 200 (489 days)	–	[96]
Electro-deposoted MnO_2@GF	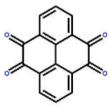	2 м H_2SO_4 + 2 м мnSO$_4$	0.3–1.3 V	210 mAh g^{-1} at 0.16 mA cm^{-2}	5000 (≈80%)	132.6/30.8	[49]
GF modified with carbon nanotube	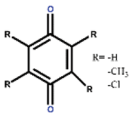	0.5 м H_2SO_4 + 1 м мnSO$_4$	0.3–1.3 V	320 mAh g^{-1} at 0.148 A g^{-1}	4000 (77%)	166.4/–	[57]
Carbon felt	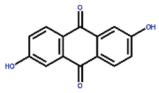	1 м H_2SO_4 + 0.5 м мnSO$_4$	0.2–1.6 V	100 mAh g^{-1} at 0.63 A g^{-1}	2600 (100%)	–	[101]
Carbon felt	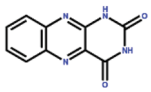	2 м HBF_4 + 2 м мn$(BF_4)_2$	1.3 V	145.5 mAh g^{-1} at 1 A g^{-1}	500 (≈100%)	110/1.650	[58]
β-мnO2	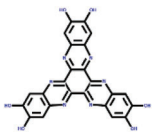	0.05 м H_2SO_4+0.2 м мnSO$_4$	0.4–1.4 V	253 mAh g^{-1} at 0.1 A g^{-1}	2000 (≈93%)	118/52.4	[103]
мnO$_2$@GF	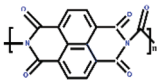	2 м H_2SO_4 + 2 м мnSO$_4$	0.5–1.7 V	77 mAh g^{-1} at 1 A g^{-1}	5000 (67.9%)	91.87/-	[110]
Indium hexacyanoferrate (InHCF)	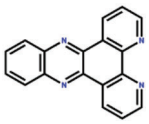	0.05 м H_2SO_4	0.2–1.5 V	37 mAh g^{-1} at 1 A g^{-1}	3000 (76.1%)	28/–	[104]
CuFePBA@мXene	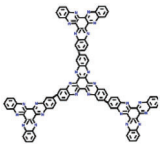	PVA-H_2SO_4	0-1.5 V	74.5 mAh cm^{-3} at 1 A cm^{-3}	10 000 (≈98.2%)	64.3 mWh cm^{-3}	[54]
Indium hexacyanoferrate (InHCF)	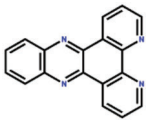	0.05 м H_2SO_4 + 1 м KCl	0.2–1.2 V	134.4 mAh g^{-1} at 1 A g^{-1}	5000 (82.5%)	–	[137]
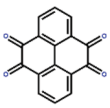	Pb	1 м H_2SO_4	0.5–1.0 V	236 mAh g^{-1} at 0.2 A g^{-1}	1000 (≈68%)	–	[114]
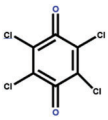	Pb	5 м H_2SO_4	0.6–1.4 V	208 mAh g^{-1} at 0.2 A g^{-1}	3000 (≈60%)	–	[112]

(*Continued*)

 © 2023 The Authors. Advanced Materials published by Wiley-VCH GmbH

15214095, 2023, 42, Downloaded from https://onlinelibrary.wiley.com/doi/10.1002/adma.202302199 by Dalian Institute Of Chemical, Wiley Online Library on [24/01/2024]. See the Terms and Conditions (https://onlinelibrary.wiley.com/terms-and-conditions) on Wiley Online Library for rules of use; OA articles are governed by the applicable Creative Commons License

Table 1. (Continued).

Cathode	Anode	Electrolyte	Out voltage	Capacity	Cycle life (retention)	Energy/power density [Wh kg^{-1}/kW kg^{-1}]	Refs.
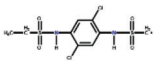	AC	1 M H_2SO_4-PVA	−0.3–0.7 V	50 mAh g^{-1} at 0.1 A g^{-1}	2000(≈90%)	–	[76]
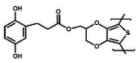	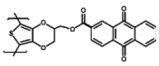	Pyridine-based proton	0–0.7 V	103 mAh g^{-1} at 0.12 A g^{-1}	–	–	[75]
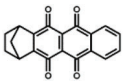		protic ionic liquid electrolyte	0.8 V	62 mAh g^{-1} at 0.12 A g^{-1}	500 (80%)	–	[120]
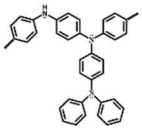	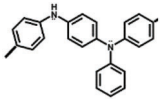	2 M HCl	1.1 V	80 mAh g^{-1} at 1 A g^{-1}	1000 (84%)	33.9/0.423	[122]
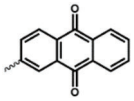	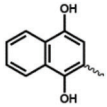	1 M H_2SO_4	0–0.9 V	78 mAh g^{-1} at 0.5 A g^{-1}	2000 (≈50%)	–	[62]
PANI@CNT	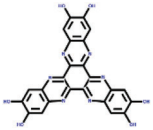	PVA–H_2SO_4	0–1.3 V	90.1 mAh cm^{-3} at 500 mA cm^{-3}	500 (≈100%)	58.5 mWh cm^{-3}	[55]
PANI on graphene paper	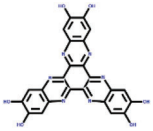	H_2SO_4–PVA	0–1.5 V	186.4 mAh g^{-1} at 0.0615 A g^{-1}	–	40.88 mWh cm^{-3}	[123]
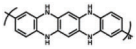	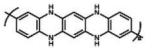	2 M $ZnSO_4$	0.2–1.2 V	147 mAh g^{-1} at 0.1 A g^{-1}	500 (94%)	–	[125]
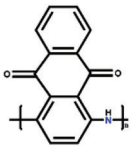	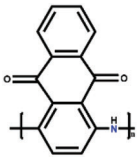	4 M H_2SO_4	0.1–1.2 V	77 mAh g^{-1} at 12 A g^{-1}	500 (70%)	–	[126]
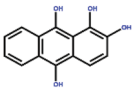	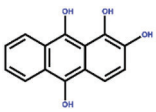	1 M H_2SO_4	1.04 V	163 mAh g^{-1} at 2.233 A g^{-1}	100 (47%)	–	[127]

1

discharge. However, due to their lightweight, organic electrodes exhibit low tap density, resulting in a lower volumetric capacity of organic electrode materials. Additionally, organic molecules are still susceptible to inevitable dissolution issues during charge–discharge processes. Polymerization of small organic molecules into polymers seems to be an effective way to solve the problem of material dissolution into electrolytes.

Although significant progress has been madein APBs, there are still challenging issues that need to be addressed in the future. Organic electrode materials typically possess a narrow potential window, which can reduce the energy density of APBs. Therefore, it is necessary to develop new organic electrode materials that contain redox-active groups with a wider operating voltage range and a higher specific capacity. This will heavily rely on the judicious structural design and morphological control of innovative organic electrode materials. Importantly, it is necessary to identify their redox potentials when novel organic electrode materials are designed. Simultaneously, molecular engineering strategies can be employed to adjust the redox potentials by introducing electron-withdrawing groups for n-type organic compounds, or

 © 2023 The Authors. Advanced Materials published by Wiley-VCH GmbH

15214095, 2023, 42, Downloaded from https://onlinelibrary.wiley.com/doi/10.1002/adma.202302199 by Dalian Institute Of Chemical, Wiley Online Library on [24/01/2024]. See the Terms and Conditions (https://onlinelibrary.wiley.com/terms-and-conditions) on Wiley Online Library for rules of use; OA articles are governed by the applicable Creative Commons License

Table 2. The advantages and disadvantages of different organic materials, electrolytes, and additive optimization.

Parameter	Type	Advantages	Disadvantages
Organic materials	n-type	1) High specific capacity; 2) high energy density.	1) Low redox potential; 2) normally high solubility.
	p-type	1) High redox potential; 2) Fast kinetics.	1) Low specific capacity
	Bipolar-type conductive polymers	1) High conductivity.	1) Low capacity; 2) sloping plateau.
Electrolytes	Aqueous acid electrolytes (e.g., H_2SO_4, H_3PO_4, etc.)	1) Low cost; 2) high ionic conductivity; 3) strong proton donating capability.	1) The dissolution of electrode materials; 2) the corrosion of electrode materials and current collectors; 3) a narrow voltage window.
	Water-in-salt	1) Reduced water activity; 2) improved stability of electrode materials; 3) extended operating voltage.	1) High cost; 2) increased electrolyte viscosity; 3) low conductivity; 4) reduced ion diffusion rate.
	Water-in-acid (concentrated H_3PO_4 electrolyte)	1) Stable cycle life; 2) fast electrode/electrolyte interfacial kinetics; 3) extremely low-melting temperature.	1) High cost; 2) the corrosion of current collectors.
	Non-aqueous (protonated pyridinium triflate derivate in acetonitrile (ACN))	1) A high working potential; 2) weak solvation capability.	1) Increased toxicity and high cost; 2) flammable materials; 3) environmental issues.
Electrolyte additives	Water-in-sugar (super-concentrated glucose)	1) Reduced water activity; 2) improve the electrode materials stability; 3) expanded operating voltage.	1) The increase of electrolyte viscosity; 2) low conductivity; 3) reduced ion diffusion rate.
	Molecular crowding electrolyte (e.g., poly(ethylene glycol), glycerol, glycine)	1) Low cost; 2) reduced water activity; 3) improved stability of electrode materials; 4) the suppression of HER (hydrogen evolution reaction); 5) expanded working potential window.	1) The diffusion of protons can be obstructed; 2) inferior rate performance; 3) low conductivity.

by utilizing other emerging molecular systems such as imine-carbonyl compounds, which can improve the output voltage and stability of organic electrode materials. In terms of the synthesis of redox-active organic molecules and their polymerization, one future direction is to avoid multiple organic synthesis steps together with the use of more environmentally compatible solvents or under solvent-free conditions. Environmental friendliness and cost-effectiveness are the two crucial factors that should always be taken into consideration. Although bipolar organic molecular systems are promising candidates for APBs, their current electrochemical performance is still limited, necessitating the development of new bipolar polymers/small molecules with advanced designs of their chemical structures. To uncover the H^+-storage mechanisms of organic materials in APBs, a deep understanding of the structure-property relationship from the perspective of the molecular level and the performance of APBs, is highly desired. In most of the discussed examples, the mass loading of the conductive additive is rather high, dramatically decreasing the amount of redox-active organic materials. Therefore, the number of conductive additives in the composition of electrodes should be minimized. The use of a conducting polymer backbone (e.g., PEDOT) can provide rapid electron transport and serve as an anchor for the redox group. This makes it a possible option for producing organic electrode materials without adding conducting additives. In addition to carbon-based materials, other 2D materials such as MXene[128,129] and black phosphorus can be promising alternatives as conductive fillers.[130–132] Moreover, the covalent functionalization of 2D materials with redox-active organic molecules can be potentially explored as well, which can provide more robust and stable electrode systems during electrochemical processes. However, the degree of covalent functionalization on 2D materials should be delicately tuned.

Moreover, as shown in **Table 2**, the rational design and engineering of electrolytes, such as water-in-salt, water-in-acid, or non-aqueous electrolytes, is significant in reducing structural degradation and capacity fading issues. With the introduction of electrolyte additives (e.g., glucose, poly(ethylene glycol), glycerol, glycine, etc.), the formation of hydrogen bonds between water and electrolyte additives results in the reduction of water activity, which favors to improve the stability of electrode materials and expand the working potential window. In addition, if the molarity/molality of the acidic electrolyte such as H_2SO_4 increases, the hydrogen bonds between the water molecules can be broken due to the interaction of SO_4^{2-} and water molecules via hydrogen bonding, which can reduce the freezing point of aqueous electrolytes (5 M H_2SO_4, −70 °C). The corrosion of electrode materials, separators, and current collectors in acidic solution needs to be paid more attention to, and it is important to develop acid- and corrosion-resistant separator materials for the development of APBs. In addition, a high concentration of salts, such as 3.5 M $Mn(ClO_4)_2$, can be utilized as an electrolyte to mitigate the corrosion of stainless steel current collectors and enhance the stability of the electrode materials.

© 2023 The Authors. Advanced Materials published by Wiley-VCH GmbH

15214095, 2023, 42, Downloaded from https://onlinelibrary.wiley.com/doi/10.1002/adma.202302199 by Dalian Institute Of Chemical, Wiley Online Library on [24/01/2024]. See the Terms and Conditions (https://onlinelibrary.wiley.com/terms-and-conditions) on Wiley Online Library for rules of use; OA articles are governed by the applicable Creative Commons License

Once the energy-storage performance is optimized further applications may be considered. To broaden the scope of their applications, more effort should be given to the fabrication and understanding of low-temperature (−40 to −70 °C) APBs which will be invaluable for end-user applications such as aerospace technologies, telecommunications, and polar expeditions, where conventional batteries may show subpar performance. In this context, the development of suitable electrolytes to meet these operating conditions is highly demanded. Design of novel all-organic APBs by making full use of the advantages of organic electrodes, for example, all-polymer-based or bio-based APBs, is an interesting direction that should be largely explored. To characterize APB-based systems, there are other emerging and promising techniques that can be considered, such as synchrotron radiation and neutron scattering spectra, as well as optical fiber sensing.[133–136] For instance, optical fiber sensing has been employed to monitor various parameters in batteries, including temperature, electrolyte density, state-of-charge, ion kinetics, oxygen concentration, and degradation process.[135,136] In terms of manufacturing techniques, 3D printing and roll-to-roll processing might be useful tools for the large-scale production of APBs.

APBs are being actively researched and developed, and hold the potential to afford a low-cost, high-energy, safe, and stable energy-storage solution. While there is still a long way to go before these batteries can be fully optimized and mass-produced for practical applications, the journey is certainly worth considering.

Acknowledgements

X.Z. would like to thank the financial support from Stiftelsen Chalmers Tekniska Högskola, Adlerbertska Forskningsstiftelsen (C2020-1230, C2021-1258), Carl Tryggers Stiftelse (CTS 22:2286), Wenner-Gren Stiftelserna (2021-0183), Swedish Foundation for International Cooperation in Research and Higher Education (IB 2020-8789), Göteborg Energi (Tänk:Om Stipendiet), Swedish Research Council Starting Grant (2020-04903), and 2D-TECH VINNOVA Competence Center (Ref. 2019-00068).

Conflict of Interest

The authors declare no conflict of interest.

Keywords

aqueous proton batteries, device design and construction, organic electrodes, proton-storage chemistry

Received: March 8, 2023
Revised: May 10, 2023
Published online: September 15, 2023

[1] D. Chao, W. Zhou, F. Xie, C. Ye, H. Li, M. Jaroniec, S. Qiao, *Sci. Adv.* **2020**, *6*, aba4098.
[2] P. Simon, Y. Gogotsi, *Nat. Mater.* **2020**, *19*, 1151.
[3] M. R. Lukatskaya, B. Dunn, Y. Gogotsi, *Nat. Commun.* **2016**, *7*, 12647.
[4] C. Lu, X. Chen, *J. Mater. Chem. A* **2021**, *9*, 753.
[5] J. Huang, K. Yuan, Y. Chen, *Adv. Funct. Mater.* **2022**, *32*, 2108107.
[6] J. Ding, W. Hu, E. Paek, D. Mitlin, *Chem. Rev.* **2018**, *118*, 6457.
[7] V. Palomares, P. Serras, I. Villaluenga, K. B. Hueso, J. Carretero-González, T. Rojo, *Energy Environ. Sci.* **2012**, *5*, 5884.
[8] K. H. Choi, J. T. Yoo, C. K. Lee, S. Y. Lee, *Energy Environ. Sci.* **2016**, *9*, 2812.
[9] E. Pomerantseva, F. Bonaccorso, X. Feng, Y. Cui, Y. Gogotsi, *Science* **2019**, *366*, 969.
[10] J. Huang, X. Dong, Z. Guo, Y. Wang, *Angew. Chem., Int. Ed.* **2020**, *59*, 18333.
[11] J. Yang, J. Cao, X. Zhao, K. Zhang, S. Zheng, Z. Gu, X. Wu, *EnergyChem* **2022**, *4*, 100092.
[12] D. Yu, R. Tian, F. Du, *Adv. Energy Sustainable Res.* **2022**, *3*, 2100207.
[13] Z. Su, M. Zhao, Q. Zheng, L. Jiao, M. Shi, M. Li, T. Xu, X. Zhao, *Electrochim. Acta* **2022**, *410*, 139792.
[14] H. Yu, C. Deng, H. Yan, M. Xia, X. Zhang, Z. B. Wang, J. Shu, *Nano-Micro Lett.* **2021**, *13*, 41.
[15] C. Yang, D. Li, H. Gao, Q. Liu, J. Zhu, F. Wang, M. Jiang, *ACS Appl. Energy Mater.* **2020**, *3*, 2674.
[16] S. Guo, G. Fang, S. Liang, M. Chen, X. Wu, *Acta Mater.* **2019**, *180*, 51.
[17] H. Dong, O. Tutusaus, Y. Liang, Y. Zhang, Z. Lebens-Higgins, W. Yang, R. Mohtadi, Y. Yao, *Nat. Energy* **2020**, *5*, 1043.
[18] P. Wang, Z. Chen, H. Wang, Z. Ji, Y. Feng, J. Wang, J. Liu, M. Hu, J. Fei, W. Gan, Y. Huang, *Energy Storage Mater.* **2020**, *25*, 426.
[19] D. Yang, Y. Zhou, H. Geng, C. Liu, B. Lu, X. Rui, Q. Yan, *Coord. Chem. Rev.* **2020**, *424*, 213521.
[20] T. Xu, D. Wang, Z. Li, Z. Chen, J. Zhang, T. Hu, X. Zhang, L. Shen, *Nano-Micro Lett.* **2022**, *14*, 126.
[21] Z. Su, J. Chen, J. Stansby, C. Jia, T. Zhao, J. Tang, Y. Fang, A. Rawal, J. Ho, C. Zhao, *Small* **2022**, *18*, 2201449.
[22] Q. Chen, J. Jin, M. Song, X. Zhang, H. Li, J. Zhang, G. Hou, Y. Tang, L. Mai, L. Zhou, *Adv. Mater.* **2022**, *34*, 2107992.
[23] M. Shi, M. Zhao, L. Jiao, Z. Su, M. Li, X. Song, *J. Power Sources* **2021**, *509*, 230333.
[24] C. Wang, S. Zhao, X. Song, N. Wang, H. Peng, J. Su, S. Zeng, X. Xu, J. Yang, *Adv. Energy Mater.* **2022**, *12*, 2200157.
[25] Y. Xu, X. Wu, X. Ji, *Small Struct.* **2021**, *2*, 2000113.
[26] S. Zhang, X. Zhao, Y. Zhang, Y. Zhao, T. Li, J. Liu, F. Huang, T. Lin, *J. Power Sources* **2022**, *550*, 232110.
[27] L. Xu, Y. Zhang, W. Zhou, F. Jiang, H. Zhang, Q. Jiang, Y. Jia, R. Wang, A. Liang, J. Xu, X. Duan, *ACS Appl. Mater. Interfaces* **2020**, *12*, 45202.
[28] Z. Song, Y. Qian, M. L. Gordin, D. Tang, T. Xu, M. Otani, H. Zhan, H. Zhou, D. Wang, *Angew. Chem., Int. Ed.* **2015**, *54*, 13947.
[29] C. Peng, X. Zhang, *Chemistry* **2021**, *3*, 873.
[30] Q. Li, M. Horn, Y. Wang, J. MacLeod, N. Motta, J. Liu, *Materials* **2019**, *12*, 703.
[31] Q. Wu, Y. Sun, H. Bai, G. Shi, *Phys. Chem. Chem. Phys.* **2011**, *13*, 11193.
[32] X. Zhang, L. Hou, A. Ciesielski, P. Samorì, *Adv. Energy Mater.* **2016**, *6*, 1600671.
[33] A. C. Ferrari, F. Bonaccorso, V. Fal'ko, K. S. Novoselov, S. Roche, P. Bøggild, S. Borini, F. H. L. Koppens, V. Palermo, N. Pugno, J. A. Garrido, R. Sordan, A. Bianco, L. Ballerini, M. Prato, E. Lidorikis, J. Kivioja, C. Marinelli, T. Ryhänen, A. Morpurgo, J. N. Coleman, V. Nicolosi, L. Colombo, A. Fert, M. Garcia-Hernandez, A. Bachtold, G. F. Schneider, F. Guinea, C. Dekker, M. Barbone, et al., *Nanoscale* **2015**, *7*, 4598.
[34] C. Backes, A. M. Abdelkader, C. Alonso, A. Andrieux-Ledier, R. Arenal, J. Azpeitia, N. Balakrishnan, L. Banszerus, J. Barjon, R. Bartali, S. Bellani, C. Berger, R. Berger, M. M. B. Ortega, C. Bernard, P. H. Beton, A. Beyer, A. Bianco, P. Bøggild, F. Bonaccorso, G. B. Barin, C. Botas, R. A. Bueno, D. Carriazo, A. Castellanos-Gomez, M.

© 2023 The Authors. Advanced Materials published by Wiley-VCH GmbH

15214095, 2023, 42, Downloaded from https://onlinelibrary.wiley.com/doi/10.1002/adma.202302199 by Dalian Institute Of Chemical, Wiley Online Library on [24/01/2024]. See the Terms and Conditions (https://onlinelibrary.wiley.com/terms-and-conditions) on Wiley Online Library for rules of use; OA articles are governed by the applicable Creative Commons License

Christian, A. Ciesielski, T. Ciuk, M. T. Cole, J. Coleman, et al., *2D Mater.* **2020**, *7*, 022001.
[35] S. Han, D. Wu, S. Li, F. Zhang, X. Feng, *Adv. Mater.* **2014**, *26*, 849.
[36] B. Guo, G. Liang, S. Yu, Y. Wang, C. Zhi, J. Bai, *Energy Storage Mater.* **2021**, *39*, 146.
[37] V. Georgakilas, M. Otyepka, A. B. Bourlinos, V. Chandra, N. Kim, K. C. Kemp, P. Hobza, R. Zboril, K. S. Kim, *Chem. Rev.* **2012**, *112*, 6156.
[38] N. An, Y. An, Z. Hu, B. Guo, Y. Yang, Z. Lei, *J. Mater. Chem. A* **2015**, *3*, 22239.
[39] H. Zhou, A. Uysal, D. M. Anjos, Y. Cai, S. H. Overbury, M. Neurock, J. K. McDonough, Y. Gogotsi, P. Fenter, *Adv. Mater. Interfaces* **2015**, *2*, 1500277.
[40] L. Hou, C. Kong, Z. Hu, Y. Yang, H. Wu, Z. Li, X. Wang, P. Yan, X. Feng, *Appl. Surf. Sci.* **2020**, *508*, 145192.
[41] K. Yang, L. Hu, Y. Wang, J. Xia, M. Sun, Y. Zhang, C. Gou, C. Jia, *J. Mater. Chem. A* **2022**, *10*, 12532.
[42] L. Jiao, F. Ma, X. Wang, Z. Li, Z. Hu, Q. Yin, *ACS Appl. Energy Mater.* **2021**, *4*, 7811.
[43] B. Yang, Y. Ma, D. Bin, H. Lu, Y. Xia, *ACS Appl. Mater. Interfaces* **2021**, *13*, 58818.
[44] X. Chen, H. Wang, H. Yi, X. Wang, X. Yan, Z. Guo, *J. Phys. Chem. C* **2014**, *118*, 8262.
[45] R. Shi, C. Han, H. Duan, L. Xu, D. Zhou, H. Li, J. Li, F. Kang, B. Li, G. Wang, *Adv. Energy Mater.* **2018**, *8*, 1802088.
[46] W. Yang, H. Yang, H. Zhou, *Batteries Supercaps* **2022**, *5*, 202200197.
[47] G. Liang, F. Mo, X. Ji, C. Zhi, *Nat. Rev. Mater.* **2021**, *6*, 109.
[48] Z. Guo, Y. Ma, X. Dong, J. Huang, Y. Wang, Y. Xia, *Angew. Chem., Int. Ed.* **2018**, *57*, 11737.
[49] Z. Guo, J. Huang, X. Dong, Y. Xia, L. Yan, Z. Wang, Y. Wang, *Nat. Commun.* **2020**, *11*, 959.
[50] Y. Chen, J. Li, Q. Zhu, K. Fan, Y. Cao, G. Zhang, C. Zhang, Y. Gao, J. Zou, T. Zhai, C. Wang, *Angew. Chem., Int. Ed.* **2022**, *61*, e202116289.
[51] T. S. Mathis, N. Kurra, X. Wang, D. Pinto, P. Simon, Y. Gogotsi, *Adv. Energy Mater.* **2019**, *9*, 1902007.
[52] S. Fleischmann, J. B. Mitchell, R. Wang, C. Zhan, D. Jiang, V. Presser, V. Augustyn, *Chem. Rev.* **2020**, *120*, 6738.
[53] C. Choi, D. S. Ashby, D. M. Butts, R. H. DeBlock, Q. Wei, J. Lau, B. Dunn, *Nat. Rev. Mater.* **2020**, *5*, 5.
[54] M. Shi, R. Wang, L. Li, N. Chen, P. Xiao, C. Yan, X. Yan, *Adv. Funct. Mater.* **2023**, *33*, 2209777.
[55] J. Xu, M. Shi, J. He, H. Ye, H. Zhu, C. Yang, L. Zhao, C. Yan, *Composites, Part B* **2022**, *235*, 109750.
[56] J. Wang, Z. Liu, H. Wang, F. Cui, G. Zhu, *Chem. Eng. J.* **2022**, *450*, 138051.
[57] X. Yang, Y. Ni, Y. Lu, Q. Zhang, J. Hou, G. Yang, X. Liu, W. Xie, Z. Yan, Q. Zhao, J. Chen, *Angew. Chem., Int. Ed.* **2022**, *61*, e202209642.
[58] T. Sun, H. Du, S. Zheng, J. Shi, Z. Tao, *Adv. Funct. Mater.* **2021**, *31*, 2010127.
[59] Z. Ye, S. Xie, Z. Cao, L. Wang, D. Xu, H. Zhang, J. Matz, P. Dong, H. Fang, J. Shen, M. Ye, *Energy Storage Mater.* **2021**, *37*, 378.
[60] Z. Song, L. Miao, H. Duan, L. Ruhlmann, Y. Lv, D. Zhu, *Angew. Chem., Int. Ed.* **2022**, *61*, 202208821.
[61] Y. Lu, Q. Zhang, L. Li, Z. Niu, J. Chen, *Chem* **2018**, *4*, 2786.
[62] X. Wang, J. Zhou, W. Tang, *Energy Storage Mater.* **2021**, *36*, 1.
[63] L. Yan, Q. Zhu, Y. Qi, J. Xu, Y. Peng, J. Shu, J. Ma, Y. Wang, *Angew. Chem., Int. Ed.* **2022**, *61*, e202211107.
[64] Y. Lin, H. Cui, C. Liu, R. Li, S. Wang, G. Qu, Z. Wei, Y. Yang, Y. Wang, Z. Tang, H. Li, H. Zhang, C. Zhi, H. Lv, *Angew. Chem., Int. Ed.* **2023**, *62*, e202218745.
[65] M. Boota, M. Bécuwe, Y. Gogotsi, *ACS Appl. Energy Mater.* **2020**, *3*, 3144.
[66] M. Yao, C. Guo, Q. Geng, Y. Zhang, X. Zhao, X. Zhao, Y. Wang, *Ind. Eng. Chem. Res.* **2022**, *61*,7480.
[67] M. Shi, R. Wang, J. He, L. Zhao, K. Dai, C. Yan, *Chem. Eng. J.* **2022**, *450*, 138238.
[68] K. Li, X. Wang, S. Li, P. Urbankowski, J. Li, Y. Xu, Y. Gogotsi, *Small* **2020**, *16*, 1906851.
[69] P. Kurzweil, *J. Power Sources* **2010**, *195*, 4424.
[70] D. Rochefort, A. L. Pont, *Electrochem. Commun.* **2006**, *8*, 1539.
[71] C. Poinsignon, M. Amarilla, F. Tedjar, *J. Mater. Chem.* **1993**, *3*, 1227.
[72] M. Minakshi, D. R. G. Mitchell, *J. Appl. Electrochem.* **2009**, *39*, 1.
[73] X. Wang, C. Bommier, Z. Jian, Z. Li, R. S. Chandrabose, I. A. Rodríguez-Pérez, P. A. Greaney, X. Ji, *Angew. Chem., Int. Ed.* **2017**, *56*, 2909.
[74] Y. Ma, Z. Guo, X. Dong, Y. Wang, Y. Xia, *Angew. Chem., Int. Ed.* **2019**, *58*, 4622.
[75] R. Emanuelsson, M. Sterby, M. Strømme, M. Sjödin, *J. Am. Chem. Soc.* **2017**, *139*, 4828.
[76] D. Shen, A. M. Rao, J. Zhou, B. Lu, *Angew. Chem., Int, Ed.* **2022**, *61*, e202201972.
[77] F. Ma, Z. Hu, L. Jiao, X. Wang, Y. Yang, Z. Li, Y. He, *Adv. Mater. Interfaces* **2021**, *8*, 2002161.
[78] M. Shi, C. Peng, X. Zhang, *Small* **2023**, *19*, 2301449.
[79] X. Wu, J. J. Hong, W. Shin, L. Ma, T. Liu, X. Bi, Y. Yuan, Y. Qi, T. W. Surta, W. Huang, J. Neuefeind, T. Wu, P. A. Greaney, J. Lu, X. Ji, *Nat. Energy* **2019**, *4*, 123.
[80] H. Yang, J. Lee, J. Y. Cheong, Y. Wang, G. Duan, H. Hou, S. Jiang, I. D. Kim, *Energy Environ. Sci.* **2021**, *14*, 4228.
[81] Y. Chen, K. Fan, Y. Gao, C. Wang, *Adv. Mater.* **2022**, *34*, 2200662.
[82] X. Deng, J. Kumankuma, G. Zhang, J. Hao, X. Zhao, L. Li, H. Li, C. Han, B. Li, *InfoMat* **2022**, *5*, 12382.
[83] Z. Tie, Z. Niu, *Angew. Chem., Int. Ed.* **2020**, *59*, 21293.
[84] M. Lee, J. Hong, B. Lee, K. Ku, S. Lee, C. B. Park, K. Kang, *Green Chem.* **2017**, *19*, 2980.
[85] F. Zhang, Y. Cheng, Z. Niu, J. Ye, G. Dai, X. Zhang, Y. Zhao, *ChemElectroChem* **2020**, *7*, 1781.
[86] R. Shi, Y. Zhao, S. Jiao, Q. Yue, G. Gu, K. Zhang, *Exploration* **2022**, *2*, 20220066.
[87] M. Li, J. Liu, Y. Li, G. Xing, X. Yu, C. Peng, L. Chen, *CCS Chem.* **2021**, *3*, 696.
[88] L. Hou, C. Kong, Z. Hu, Y. Han, B. Wu, *J. Electroanal. Chem.* **2021**, *895*, 115402.
[89] Z. Tie, L. Liu, S. Deng, D. Zhao, Z. Niu, *Angew. Chem., Int. Ed.* **2020**, *59*, 4920.
[90] N. Wang, Z. Guo, Z. Ni, J. Xu, X. Qiu, J. Ma, P. Wei, Y. Wang, *Angew. Chem., Int. Ed.* **2021**, *60*, 20826.
[91] Q. Jiang, N. Kurra, M. Alhabeb, Y. Gogotsi, H. N. Alshareef, *Adv. Energy Mater.* **2018**, *8*, 1703043.
[92] S. Dutta, S. Pal, S. De, *New J. Chem.* **2019**, *43*, 12385.
[93] W. Xu, K. Zhao, X. Liao, C. Sun, K. He, Y. Yuan, W. Ren, J. Li, *J. Am. Chem. Soc.* **2022**, *144*, 17407.
[94] X. Mu, D. Wang, F. Du, G. Chen, C. Wang, Y. Wei, Y. Gogotsi, Y. Gao, Y. Dall'Agnese, *Adv. Funct. Mater.* **2019**, *29*, 1902953.
[95] T. Xu, Z. Li, D. Wang, M. Zhang, L. Ai, Z. Chen, J. Zhang, X. Zhang, L. Shen, *Adv. Funct. Mater.* **2022**, *32*, 2107720.
[96] H. Guo, L. Wan, J. Tang, S. Wu, Z. Su, N. Sharma, *Nano Energy* **2022**, *102*, 107642.
[97] Z. Liu, L. Qin, B. Lu, X. Wu, S. Liang, J. Zhou, *ChemSusChem* **2022**, *15*, 202200348.
[98] T. Nokami, T. Matsuo, Y. Inatomi, N. Hojo, T. Tsukagoshi, H. Yoshizawa, A. Shimizu, H. Kuramoto, K. Komae, H. Tsuyama, J. I. Yoshida, *J. Am. Chem. Soc.* **2012**, *134*, 19694.
[99] S. Wu, J. Chen, Z. Su, H. Guo, T. Zhao, C. Jia, J. Stansby, J. Tang, A. Rawal, Y. Fang, J. Ho, C. Zhao, *Small* **2022**, *18*, 2202992.
[100] Z. Su, J. Tang, J. Chen, H. Guo, S. Wu, S. Yin, T. Zhao, C. Jia, Q. Meyer, A. Rawal, J. Ho, Y. Fang, C. Zhao, *Small Struct.* **2023**, *4*, 2200257.

© 2023 The Authors. Advanced Materials published by Wiley-VCH GmbH

15214095, 2023, 42, Downloaded from https://onlinelibrary.wiley.com/doi/10.1002/adma.202302199 by Dalian Institute Of Chemical, Wiley Online Library on [24/01/2024]. See the Terms and Conditions (https://onlinelibrary.wiley.com/terms-and-conditions) on Wiley Online Library for rules of use; OA articles are governed by the applicable Creative Commons License

[101] J. Yu, J. Li, Z. Y. Leong, D. sheng Li, J. Lu, Q. Wang, H. Y. Yang, *Mater. Today Energy* **2021**, *22*, 100872.
[102] G. Sun, B. Yang, X. Chen, Y. Wei, G. Yin, H. Zhang, Q. Liu, *Chem. Eng. J.* **2022**, *431*, 134253.
[103] Y. Dai, X. Yan, J. Zhang, C. Wu, Q. Guo, J. Luo, M. Hu, J. Yang, *Electrochim. Acta* **2023**, *442*, 141870.
[104] J. Qiao, M. Qin, Y. M. Shen, J. Cao, Z. Chen, J. Xu, *Chem. Commun.* **2021**, *57*, 4307.
[105] S. Qiu, Y. Xu, X. Li, S. K. Sandstrom, X. Wu, X. Ji, *Electrochem. Commun.* **2021**, *122*, 106880.
[106] H. Jiang, W. Shin, L. Ma, J. J. Hong, Z. Wei, Y. Liu, S. Zhang, X. Wu, Y. Xu, Q. Guo, M. A. Subramanian, W. F. Stickle, T. Wu, J. Lu, X. Ji, *Adv. Energy Mater.* **2020**, *10*, 2000968.
[107] C. Strietzel, K. Oka, M. Strømme, R. Emanuelsson, M. Sjödin, *ACS Appl. Mater. Interfaces* **2021**, *13*, 5349.
[108] T. Sun, Q. Nian, H. Du, S. Zheng, D. Han, Z. Tao, *J. Mater. Chem. A* **2022**, *10*, 17288.
[109] W. Liu, Z. Zhang, J. Shi, Y. Zheng, Y. Wu, X. Fu, N. Liu, J. Su, Y. Gao, *J. Mater. Chem. A* **2022**, *10*, 4043.
[110] W. Han, M. Li, Y. Ma, J. Yang, *Electrochim. Acta* **2022**, *403*, 139550.
[111] B. P. P. Lopes, V. R. Stamenkovic, *Science* **2020**, *369*, 923.
[112] F. Yue, Z. Tie, S. Deng, S. Wang, M. Yang, Z. Niu, *Angew. Chem., Int. Ed.* **2021**, *60*, 13882.
[113] T. Sun, X. Yuan, K. Wang, S. Zheng, J. Shi, Q. Zhang, W. Cai, J. Liang, Z. Tao, *J. Mater. Chem. A* **2021**, *9*, 7042.
[114] F. Yue, Z. Tie, Y. Zhang, S. Bi, Y. Wang, Z. Niu, *Angew. Chem., Int. Ed.* **2022**, *61*, e202208513.
[115] A. Jouhara, N. Dupré, A. C. Gaillot, D. Guyomard, F. Dolhem, P. Poizot, *Nat. Commun.* **2018**, *9*, 4401.
[116] Y. Liang, Y. Jing, S. Gheytani, K. Y. Lee, P. Liu, A. Facchetti, Y. Yao, *Nat. Mater.* **2017**, *16*, 841.
[117] A. Wild, M. Strumpf, B. Häupler, M. D. Hager, U. S. Schubert, *Adv. Energy Mater.* **2017**, *7*, 1601415.
[118] T. Li, L. Wang, J. Li, *Chem. Eng. J.* **2022**, *442*, 136232.
[119] C. Strietzel, M. Sterby, H. Huang, M. Strømme, R. Emanuelsson, M. Sjödin, *Angew. Chem., Int. Ed.* **2020**, *59*, 9631.
[120] H. Wang, R. Emanuelsson, C. Karlsson, P. Jannasch, M. Strømme, M. Sjödin, *ACS Appl. Mater. Interfaces* **2021**, *13*, 19099.
[121] M. Zhu, L. Zhao, Q. Ran, Y. Zhang, R. Peng, G. Lu, X. Jia, D. Chao, C. Wang, *Adv. Sci.* **2022**, *9*, 2103896.
[122] K. C. S. Lakshmi, B. Vedhanarayanan, H. Y. Cheng, X. Ji, H. H. Shen, T. W. Lin, *J. Colloid Interface Sci.* **2022**, *619*, 123.
[123] M. Shi, J. He, Y. Zhao, L. Zhao, K. Dai, C. Yan, *Mater. Des.* **2022**, *222*, 111043.
[124] A. M. Navarro-Suárez, J. Carretero-González, T. Rojo, M. Armand, *J. Mater. Chem. A* **2017**, *5*, 23292.
[125] Z. Tie, S. Deng, H. Cao, M. Yao, Z. Niu, J. Chen, *Angew. Chem., Int. Ed.* **2022**, *61*, e202115180.
[126] T. Sun, H. Du, S. Zheng, J. Shi, X. Yuan, L. Li, Z. Tao, *Small Methods* **2021**, *5*, 2100367.
[127] L. Tong, Y. Jing, R. G. Gordon, M. J. Aziz, *ACS Appl. Energy Mater.* **2019**, *2*, 4016.
[128] S. Thurakkal, X. Zhang, *Mater. Chem. Front.* **2022**, *6*, 561.
[129] J. Tang, T. Mathis, X. Zhong, X. Xiao, H. Wang, M. Anayee, F. Pan, B. Xu, Y. Gogotsi, *Adv. Energy Mater.* **2021**, *11*, 2003025.
[130] S. Thurakkal, X. Zhang, *Mater. Chem. Front.* **2021**, *5*, 2824.
[131] S. Thurakkal, D. Feldstein, R. Perea-Causín, E. Malic, X. Zhang, *Adv. Mater.* **2021**, *33*, 2005254.
[132] S. Thurakkal, X. Zhang, *Adv. Sci.* **2020**, *7*, 1902359.
[133] Y. Ren, X. Zuo, *Small Methods* **2018**, *2*, 1800064.
[134] D. Atkins, E. Capria, K. Edström, T. Famprikis, A. Grimaud, Q. Jacquet, M. Johnson, A. Matic, P. Norby, H. Reichert, J. P. Rueff, C. Villevieille, M. Wagemaker, S. Lyonnard, *Adv. Energy Mater.* **2022**, *12*, 2102694.
[135] R. Wang, H. Zhang, Q. Liu, F. Liu, X. Han, X. Liu, K. Li, G. Xiao, J. Albert, X. Lu, T. Guo, *Nat. Commun.* **2022**, *13*, 547.
[136] G. Han, J. Yan, Z. Guo, D. Greenwood, J. Marco, Y. Yu, *Renewable Sustainable Energy Rev.* **2021**, *150*, 111514.
[137] J. Qiao, Z. Liu, Z. Wang, M. Qin, Y. Shi, J. Xu, Z. Chen, J. Cao, *ACS Appl. Energy Mater.* **2021**, *4*, 4903.

Mangmang Shi is a visiting scholar under the supervision of Prof. Xiaoyan Zhang at Chalmers University of Technology, Sweden. His current scientific interests mainly focus on the preparation of high-performance electrode materials for applications in aqueous energy-storage devices including aqueous asymmetric supercapacitors and APBs.

© 2023 The Authors. Advanced Materials published by Wiley-VCH GmbH

15214095, 2023, 42, Downloaded from https://onlinelibrary.wiley.com/doi/10.1002/adma.202302199 by Dalian Institute Of Chemical, Wiley Online Library on [24/01/2024]. See the Terms and Conditions (https://onlinelibrary.wiley.com/terms-and-conditions) on Wiley Online Library for rules of use; OA articles are governed by the applicable Creative Commons License

Xiaoyan Zhang is currently an Associate Professor at Chalmers University of Technology, Sweden. He received his Ph.D. degree from the University of Groningen, The Netherlands, followed by post-doctoral research at the University of Strasbourg, France. His research team at Chalmers is focusing on the synthesis of functional organic molecules and chemical functionalization of 2D materials for applications in high-performance energy-storage devices.

© 2023 The Authors. Advanced Materials published by Wiley-VCH GmbH

15214095, 2023, 42, Downloaded from https://onlinelibrary.wiley.com/doi/10.1002/adma.202302199 by Dalian Institute Of Chemical, Wiley Online Library on [24/01/2024]. See the Terms and Conditions (https://onlinelibrary.wiley.com/terms-and-conditions) on Wiley Online Library for rules of use; OA articles are governed by the applicable Creative Commons License